processes

MDPI

Article

Techno-Economic Optimization of a Hybrid Renewable Energy System with Seawater-Based Pumped Hydro, Hydrogen, and Battery Storage for a Coastal Hotel

Tuba Tezer [1,2]

[1] Balıkesir Vocational School, Balıkesir University, Balıkesir 10145, Türkiye; tuba.tezer@balikesir.edu.tr
[2] Renewable Energy Research, Application and Development Center, Balıkesir University, Balıkesir 10145, Türkiye

Abstract

This study presents the design and techno-economic optimization of a hybrid renewable energy system (HRES) for a coastal hotel in Manavgat, Türkiye. The system integrates photovoltaic (PV) panels, wind turbines (WT), pumped hydro storage (PHS), hydrogen storage (electrolyzer, tank, and fuel cell), batteries, a fuel cell-based combined heat and power (CHP) unit, and a boiler to meet both electrical and thermal demands. Within this broader optimization framework, six optimal configurations emerged, representing grid-connected and standalone operation modes. Optimization was performed in HOMER Pro to minimize net present cost (NPC) under strict reliability (0% unmet load) and renewable energy fraction (REF > 75%) constraints. The grid-connected PHS–PV–WT configuration achieved the lowest NPC ($1.33 million) and COE ($0.153/kWh), with a renewable fraction of ~96% and limited excess generation (~21%). Off-grid PHS-based and PHS–hydrogen configurations showed competitive performance with slightly higher costs. Hydrogen integration additionally provides complementary storage pathways, coordinated operation, waste heat utilization, and redundancy under component unavailability. Battery-only systems without PHS or hydrogen storage resulted in 37–39% higher capital costs and ~53% higher COE, confirming the economic advantage of long-duration PHS. Sensitivity analyses indicate that real discount rate variations notably affect NPC and COE, particularly for battery-only systems. Component cost sensitivity highlights PV and WT as dominant cost drivers, while PHS stabilizes system economics and the hydrogen subsystem contributes minimally due to its small scale. Overall, these results confirm the techno-economic and environmental benefits of combining seawater-based PHS with optional hydrogen and battery storage for sustainable hotel-scale applications.

Keywords: hybrid renewable energy system; pumped hydro storage; hydrogen energy storage; battery storage; cost of energy; waste heat recovery; combined heat and power (chp); techno-economic optimization

Academic Editors: Gerasimos Lyberatos, Leonidas Matsakas and Nikolaos A. Diangelakis

Received: 22 September 2025
Revised: 13 October 2025
Accepted: 16 October 2025
Published: 18 October 2025

Citation: Tezer, T. Techno-Economic Optimization of a Hybrid Renewable Energy System with Seawater-Based Pumped Hydro, Hydrogen, and Battery Storage for a Coastal Hotel. *Processes* **2025**, *13*, 3339. https://doi.org/10.3390/pr13103339

1. Introduction

In recent years, global energy demand has shown a substantial and accelerating increase due to population growth and technological advancements [1]. This demand is predominantly met through fossil fuels, which account for approximately 85% of global electricity production and are among the primary sources of greenhouse gas emissions [2]. The strong link between fossil fuel consumption and climate change underscores the urgent

need for a transition to sustainable energy systems [3]. However, solar and wind generation are inherently variable and weather-dependent, which can create temporal mismatches between supply and demand and thus hinder continuous, reliable electricity delivery. To overcome these limitations, storage and conversion technologies play a critical role in increasing renewable energy utilization and enhancing system flexibility [4]. Accordingly, the shift towards sustainable systems that incorporate renewable energy sources and reliable energy storage solutions has become imperative.

In this context, research on HRES has attracted growing attention in recent years. While earlier studies mainly focused on off-grid HRES configurations, recent research has increasingly addressed grid-connected systems supported by various energy storage technologies. These systems facilitate the integration of variable renewable energy sources into the grid and, when combined with appropriate storage options, enhance grid stability and reliability. A range of energy storage technologies exist, such as batteries, supercapacitors, hydrogen storage systems and PHS, each offering distinct technical and operational advantages [5,6]. Among these, hydrogen-based systems [2] and PHS solutions [7] have gained significant traction in recent years due to their sustainability and reliability benefits.

Among various HRES configurations, PV and hydrogen-based systems are drawing increasing interest for their potential to provide long-term energy storage and enhance overall system autonomy. Fuel cells primarily convert hydrogen into electricity through electrochemical reactions, during which a notable amount of heat is also released as a by-product. Integrating FCs with CHP functionality allows this waste heat to be recovered and utilized, thereby improving both system efficiency and overall cost-effectiveness. For instance, Hosseini et al. [8] designed a residential hybrid system consisting of PV panels, an electrolyzer, and a fuel cell, and conducted energy and exergy analyses. By incorporating a heat recovery unit composed of a steam generator and an absorption chiller that utilized thermal energy from solid oxide fuel cell (SOFC) flue gas, they met the thermal load of the residence and improved overall system efficiency. Zafar and Dincer [9] analyzed a PV/T–fuel cell system designed to co-produce electricity, heat, hydrogen, and potable water. Their results showed that utilizing fuel cell waste heat improved energy and exergy efficiencies, while the recovery of water enhanced the system's overall economic performance.

In addition, many studies in the literature have examined the use of wind and PV technologies in combination with hydrogen storage. One such study was conducted by Devrim and Bilir [10] who investigated the performance of a hybrid system and demonstrated that it could meet the annual electricity demand of a residential building in the İncek region of Ankara, with the exception of November. On the other hand, HRES configurations that integrate battery storage technologies are also extensively covered in the literature. Pürlü et al. [11] designed and optimized six HRESs, including combinations of PV panels, WT, diesel generators, batteries, and converters, for electrifying a 100-household area in Sarayköy, Türkiye, using HOMER software. The study found that the most economical system was a grid-connected PV-only configuration, while the most cost-effective off-grid system included PV, wind, and batteries.

In addition to battery and hydrogen-based storage options, PHS systems have also gained significant attention in HRES studies due to their long lifetime, low maintenance requirements, large energy storage capacity, and environmentally friendly characteristics [12,13].

Anagnostopoulos and Papantonis [14] developed a numerical method for the optimal sizing of PHS components to recover wind energy curtailed due to grid limitations. Using real data from the island of Crete, their case study demonstrated that optimized system design plays a critical role in the technical and economic viability of such configurations.

Apart from wind-based applications, PHS has also been examined in PV-based systems. For instance, Ma et al. [15] conducted a sizing optimization for an off-grid hybrid system consisting of PV panels and a PHS unit. Their findings confirmed the effectiveness of PHS in enhancing energy autonomy, particularly in remote areas.

Beyond individual PV–PHS or wind–PHS configurations, several studies have investigated hybrid systems that simultaneously integrate PV, wind, and PHS components to enhance energy autonomy and system resilience. For instance, Jurazs et al. [16] proposed a mathematical model to optimize a district-scale solar–wind–PHS system, introducing a Local Consumption Index (LCI) to account for grid-related costs. Their results revealed that LCI facilitates higher renewable integration, and that PV and wind technologies remain cost-effective even under low carbon pricing conditions. Similarly, Simão and Ramos [17] developed a multi-criteria evaluation method to optimize hybrid renewable systems combining wind, PV, and PHS. Their simulations assessed various design configurations and component capacities, identifying a technically and economically optimal solution that meets 72% of the annual energy demand. The study demonstrated that coupling PHS with PV and wind improves system flexibility, reliability, and autonomy while maintaining competitive costs.

In addition to typical PV–wind–PHS setups, other studies have investigated more complex hybrid systems incorporating additional generation and control components. For example, Pattnaik et al. [12] investigated a wind–PV–thermal hybrid system integrated with PHS and a static synchronous compensator (STATCOM) under a security-constrained optimal power flow framework. Their findings indicated that PHS significantly reduced fossil fuel dependence and operational costs, while the inclusion of STATCOM enhanced voltage stability—resulting in a 10–16% improvement in voltage profile and notable annual cost savings.

Beyond these configurations, researchers have also explored standalone HRESs integrating PV, wind, PHS, and batteries to further enhance reliability, storage flexibility, and energy autonomy. For instance, Gioutsos et al. [18] analyzed cost-optimal configurations of renewable-based systems including PV, wind, pumped hydro, and batteries for several island case studies, revealing that high renewable penetrations (up to 80%) can significantly reduce electricity generation costs. Similarly, Guezgouz et al. [19] developed a hybrid energy management strategy combining battery storage for short-term and PHS for long-term use in a solar- and wind-based off-grid system located on a farmstead in Algeria. The results indicated high reliability (97.5%) at a relatively low cost (€0.162/kWh), albeit with some sensitivity to environmental variations. Samatar et al. [20] assessed various standalone HRES configurations for a coastal area in Somalia, incorporating PV, WT, diesel generators, pumped hydro, and batteries. Their analysis using HOMER Pro and MATLAB showed that the PV–wind–PHS configuration delivered the most cost-effective and environmentally sustainable outcome, achieving a 100% renewable fraction and an LCOE of $0.03845/kWh. In a related study, Dufo-López and Lujano-Rojas [21], proposed a metaheuristic–stochastic optimization method for sizing and energy management of a standalone PV–wind–diesel system integrated with hybrid pumped hydro and battery storage, addressing renewable intermittency and system uncertainty.

In addition to standalone systems, grid-connected HRESs incorporating PV, wind, PHS, and/or batteries have also been extensively studied to improve grid stability, reduce fossil fuel dependency, and optimize operational costs. Abdelshafy et al. [22] developed an energy management strategy for a grid-connected system combining battery and pumped-storage hydropower (PSH) in the Suez region of Egypt. Using NSGA-II to minimize investment cost and CO_2 emissions, their PV and wind-based system achieved a 22.2% reduction in electricity cost and limited annual energy exchange with the national grid to

just 5%. Another notable study by Ramos et al. [23] developed an optimized scheduling model for integrating PHS with PV and wind in a grid-connected hybrid system. Their results showed significant reductions in operating costs and CO_2 emissions, reaching up to 84% during summer. The study also reported favorable financial indicators, such as a payback period of five years, demonstrating the economic and environmental benefits of using PSH in HRESs.

In recent years, there has been a growing academic interest in the potential of PHS systems in Türkiye, and several pioneering studies have been conducted. Taşcıkaraoğlu and Erdinç [24] conducted an optimization study on a wind–PHS power system that considers day-ahead and balancing markets to maximize profit by exploiting electricity price fluctuations. Based on simulation studies using real wind and market data, the proposed price-based energy management strategy integrated with pumped-hydro storage has been shown to be both effective and practically feasible for increasing economic gains and enhancing system support in high-power applications. Kocaman [25] proposes a two-stage stochastic programming model to optimize the sizing of hybrid energy systems integrating solar power with both pure and mixed types of PHS. In this model, pure PHS refers to closed-loop systems without natural water inflow, whereas mixed PHS allows natural inflow. Both configurations are evaluated under resource and demand uncertainty, with the first application presented for Türkiye. Similarly, Kumcu [26] investigated the locations and topography of dams and lakes of Türkiye to decide the feasibility, sustainability, efficiency, and environmentalism of the projects. Unlike previous studies, Saltuk [27] presents a preliminary feasibility analysis of a planned PHS project at the Gökçekaya Dam in Türkiye, focusing on its economic and technical viability. A comparison between a standalone PHS setup and one integrated with solar energy shows that hybrid support significantly shortens the payback period. The study concludes that combining PHS with solar energy and appropriate market pricing can make the investment more feasible in Turkey. Finally, Yurter et al. [28] developed two-stage stochastic programming models for closed-loop and open-loop PHS systems and conducted system sizing and cost analyses. The results demonstrated that using PHS significantly reduces investment costs and demand mismatches compared to conventional hydropower systems.

Unlike many studies conducted on general PHS systems in Türkiye, Ünver et al. [29] specifically focus on pumped-storage hydroelectric power plants (PSHPPs) in their research. They examined PSHPPs worldwide and investigated the technical and legal infrastructure required for the installation of these systems in Türkiye. Similarly, Sertkaya et al. [30] discussed the evolution of PHS systems from their conventional role in meeting peak demand to their modern function in integrating renewable energy and enabling flexible daily operation. The study highlighted that Turkey's demand for PHS has become increasingly critical, paralleling its expanding investments in nuclear and renewable energy sources. Another study on PSHPP in Türkiye was conducted by Gürsakal and Uyumaz [31]. They examine the planning stage of PSHPPs in Turkey and emphasize the importance of profitability analysis and determination of operating hours based on hourly electricity market prices. Their Relative Profitability Analysis Approach (RPAA) evaluates profitability ratios and optimizes installed capacity and energy production, providing critical parameters for effective PSHPP system design and operation.

Alongside numerous techno-economic optimization studies integrating PHS into HRES, there are also comparative works that evaluate different storage technologies such as hydrogen, batteries, and PHS within these systems. For example, Awan et al. [32] analyzed nine off-grid HRES scenarios in Sharurah, Saudi Arabia, where batteries, hydrogen, and PHS were used individually as alternative storage options. The PV-diesel-battery system showed the best techno-economic performance. However, all but one scenario includes

diesel backup, with the optimal system based on a configuration supported by fossil fuels rather than PHS or hydrogen storage. In contrast, Alili et al. [33] presented an integrated approach by combining hydrogen storage with PHS, and evaluated the impact of a hydrogen energy storage (HES) unit comprising an electrolyzer, hydrogen tank, and fuel cell within a PV/PSH-based off-grid energy system. Although the HES subsystem had relatively small capacity, it contributed to reducing excess electricity supply by 15.3% and led to a 5.4% increase in exergy efficiency. Furthermore, the inclusion of HES allowed for downsizing the PV and PSH components and resulted in a 0.5% total cost reduction.

As summarized in Table 1, earlier studies generally focused on single or dual storage configurations (e.g., battery only, PHS only, hydrogen only, battery–PHS, battery–hydrogen, PHS–hydrogen), with limited evaluation of interactions among electrical, mechanical, and hydrogen-based storage. In this work, three different storage technologies (PHS, battery, and hydrogen-based hybrid energy storage) were simultaneously defined as design variables within the same optimization model, enabling the exploration of six distinct hybrid configurations. Additionally, this HRES model includes a fuel cell-supported heat recovery unit to meet thermal demands. Although the optimal results did not include all three storages concurrently, the analysis reveals the techno-economic interactions and trade-offs that determine the competitiveness of each storage combination.

Table 1. Comparison of hybrid renewable system studies showing the evolution from single- to multi-storage configurations.

Reference	System Configuration	Storage Types	Heat Recovery/Thermal Integration	Key Limitation/Gap
Hosseini et al. [8]	PV–Electrolyzer–FC-HT	Hydrogen	SOFC-CHP	Single storage; no PHS; no CHP coupling
Pürlü et al. [11]	PV–Wind–Battery–DG	Battery	No	Single storage; no PHS; no CHP coupling
Pattnaik et al. [12]	Wind–PV–Thermal–PHS	PHS	Partial (thermal)	Single storage; no CHP coupling
Ma et al. [15]	PV–PHS	PHS	No	Single storage; no CHP coupling
Jurazs et al. [16]	PV–Wind–PHS	PHS	No	Single storage; No CHP coupling
Simão and Ramos [17]	PV–Wind–PHS	PHS	No	Single storage; no CHP coupling
Gioutsos et al. [18]	PV–Wind–PHS–Battery	PHS, Battery	No	No hydrogen storage; no CHP coupling
Guezgouz et al. [19]	PV–Wind–PHS–Battery	PHS, Battery	No	No hydrogen storage; no CHP coupling
Samatar et al. [20]	PV–Wind–Diesel–PHS–Battery	PHS, Battery	No	No hydrogen storage; no CHP coupling
Dufo-López & Lujano-Rojas [21]	PV–Wind–Diesel–PHS–Battery	PHS, Battery	No	No hydrogen storage; no CHP coupling
Abdelshafy et al. [22]	Grid-connected PV–Wind–Battery–PHS	PHS, Battery	No	No hydrogen storage; no CHP coupling
Ramos et al. [23]	Grid-connected PV–Wind–PHS	PHS	No	Single storage; no CHP coupling

Table 1. *Cont.*

Reference	System Configuration	Storage Types	Heat Recovery/Thermal Integration	Key Limitation/Gap
Awan et al. [32]	PV–Wind–Diesel (nine scenarios with single storage)	Battery/PHS/H_2 (evaluated individually)	No	Evaluated individually; Single storage; no CHP coupling
Alili et al. [33]	PV–PHS–Electrolyzer–FC-HT	PHS, Hydrogen	FC waste heat recovery	Only PV-based; no battery storage
This study	(grid connected or off grid) PV–Wind–PHS–Battery–Electrolyzer–FC-HT–FC-CHP	PHS, Battery, Hydrogen	FC waste heat recovery	Triple storage option and CHP coupling

This study further expands the analysis by integrating the identified storage technologies into both grid-connected and off-grid HRES architectures. Through the broader optimization framework, multiple hybrid configurations were systematically evaluated to capture the interactions, complementarities, and trade-offs among electrical, mechanical, and hydrogen-based storage. In addition, extensive sensitivity analyses were performed to assess how variations in component costs, load profiles, and meteorological conditions influence overall system performance and resilience, offering deeper insight into long-term feasibility.

Novelty and Contributions

Accordingly, the novelty and contributions of this study can be summarized as follows:

- This study proposes a novel HRES configuration that simultaneously investigates three storage technologies (PHS, hydrogen, batteries) with CHP-based heat recovery.
- The broader search space allowed six distinct system configurations to be obtained and analyzed in detail, showing how the inclusion or exclusion of each storage option influences system performance, levelized cost, and excess energy utilization.
- It demonstrates the practical applicability of seawater-based PHS by using the sea as the lower reservoir in a coastal hotel case study.
- The system not only addresses electrical loads but also incorporates thermal load coverage through fuel cell waste heat recovery, offering a comprehensive evaluation of hotel-scale energy systems.
- Representative values for PHS were selected based on regional topography and comparable coastal seawater PHS projects, ensuring technical and economic relevance.
- The analysis extends beyond cost optimization by evaluating financial robustness under varying discount rates and component costs, as well as the sensitivity of system economics to load and meteorological variations.

2. Methodology

To investigate the optimal design of the proposed HRES, both grid-connected and off-grid operation modes were considered. The methodology involved defining key input parameters, decision variables, and system constraints, which were then implemented in the HOMER Pro software, Version 3.14.2 (HOMER Energy LLC, Boulder, CO, USA) for optimization and performance analysis. The HRES configuration, comprising PV, WT, a PHS unit, a fuel cell, an electrolyzer, a hydrogen storage tank, and battery banks, was designed to meet the electrical and thermal energy demands of a seaside hotel located in the Manavgat district of Turkey's Mediterranean region. Owing to its coastal topography,

the sea was utilized as the lower reservoir in the PHS system, offering a practical and space-efficient design solution. The schematic representation and detailed structure of the system components are illustrated in Figure 1 and described in the following subsection.

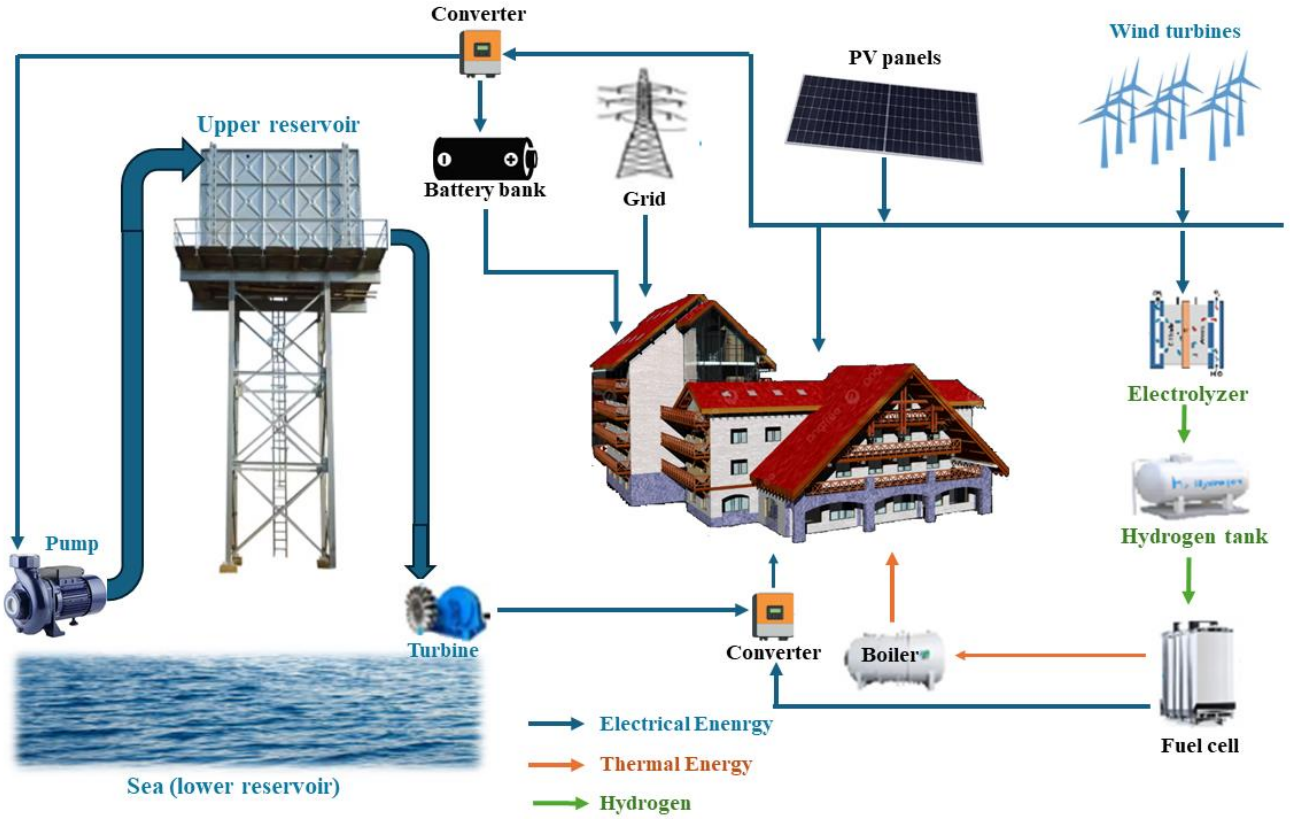

Figure 1. Overview of the hybrid PHS–hydrogen energy system.

2.1. System Configuration and Dispatch Strategy

The schematic layout of the proposed HRES is presented in Figure 1. In this system, PV panels and WT are employed for renewable electricity generation. The energy management is based on the load following dispatch strategy defined in HOMER Pro software, which prioritizes supplying energy from renewable sources and available storage units.

When surplus energy is generated, it is first stored in a PHS system. Taking advantage of the hotel's coastal location, the sea is used as the lower reservoir in the PHS configuration. If the upper reservoir is full, the excess electricity is converted into hydrogen via an electrolyzer and stored in a hydrogen tank. Additionally, a battery storage system is included to support short-term energy balancing and to compensate for sudden variations in energy demand or renewable generation.

The stored hydrogen is later used in a fuel cell to generate both electricity and heat. The waste heat produced by the fuel cell is recovered through a heat recovery system and used to meet part of the hotel's thermal load, while the remaining thermal demand is met by a natural gas boiler.

In this study, different HRES scenarios are constructed by considering three distinct storage technologies (PHS, hydrogen, and battery), along with both grid-connected and off-grid operation modes. The main objective is to analyze these configurations to identify the lowest-cost optimal solutions under reliability and renewable energy penetration constraints, with a particular focus on the performance of various storage strategies.

2.2. Meteorological Data and Load Profiles

Hourly meteorological data for the installation site were obtained from the "NASA Surface Meteorology and Solar Energy" database integrated within the HOMER Pro™ software. The long-term monthly averages of global horizontal radiation for the period 1983–2005, as well as wind speed at 50 m height and ambient temperature for the period 1984–2013, were obtained from the NASA POWER database through HOMER Pro corresponding to the geographical coordinates (36.75° N, 31.25° E) [34]. The annual wind speed and solar radiation-average temperature values for the region are presented in Figures 2 and 3, respectively.

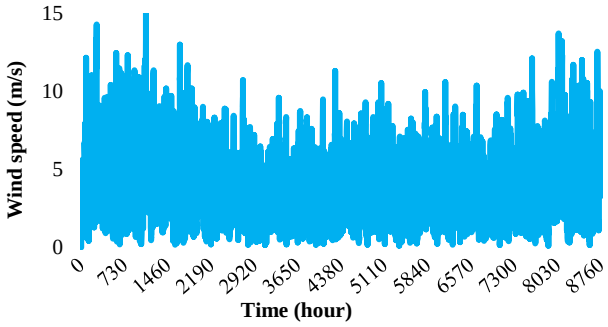

Figure 2. Hourly wind speed profile for the selected location.

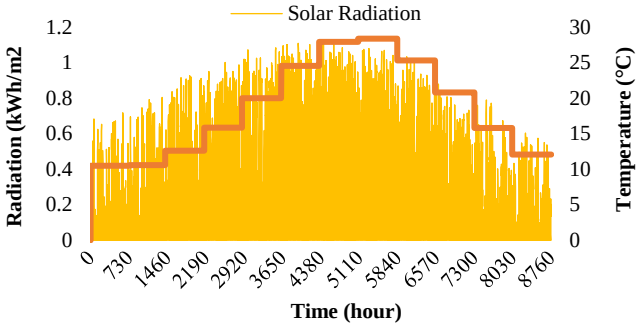

Figure 3. Hourly variation in solar radiation and ambient temperature throughout the year.

The annual electrical and thermal load profiles of the hotel were derived from a medium-sized hotel scenario located in a Mediterranean climate zone classified as "Csa" according to the Köppen climate classification, available in the HOMER library. Electrical demand increases during the summer months, while thermal energy demand is more prominent in the winter. This variation requires seasonal optimization of the energy production-consumption balance in the system design. The annual electrical and thermal load profiles are shown in Figures 4 and 5, respectively.

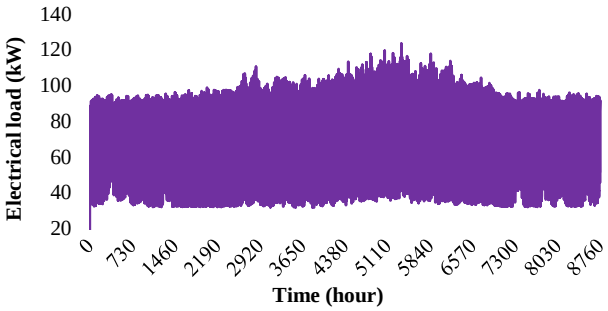

Figure 4. Annual electrical load profile.

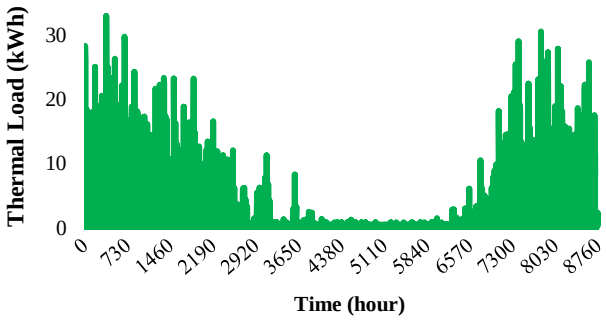

Figure 5. Annual thermal load profile.

2.3. Mathematical Model of System Components

2.3.1. PV Model

The PV panel model used in this study is a flat-plate SunPower E20-327 type panel, included in the HOMER library [34]. No tracking technology is applied. The economic lifetime of the PV modules is assumed to be 25 years. The power output of the PV (P_{PV}) can be calculated by the following Equation (1):

$$P_{PV} = P_{PV\_rated} \times f_{dr} \times \frac{G}{G_{STC}} \times (1 + \alpha_t \times (T_c - T_{STC})) \quad (1)$$

In this equation, P_{PV_rated} is the rated power capacity of the PV array under standard test conditions, and f_{dr} is the derating factor that accounts for system losses. The term G/G_{STC} adjusts the power output based on the current solar irradiance G relative to the standard test condition irradiance G_{STC}, typically 1 kW/m^2. The temperature correction factor $1 + \alpha_t \times (T_c - T_{STC})$ accounts for the change in power output due to the difference between the current cell temperature T_c and the standard temperature T_{STC} (usually 25 °C). Here, α_t is the temperature coefficient of power, representing the percentage power change per degree Celsius. In this study, the temperature coefficient of power α_t is $-0.380\%/°C$, and the derating factor f_{dr} is 88%.

The cell temperature T_c is estimated using the following Equation (2):

$$T_c = T_a + \left(\frac{T_{c,NOCT} - T_{a,NOCT}}{G_{T,NOCT}} \right) \times G_T \times \left(1 - \frac{\eta_c}{\tau\alpha} \right) \quad (2)$$

where $T_{c,NOCT}$ is the nominal operating cell temperature provided by manufacturers, typically defined under 800 W/m^2 solar irradiance ($G_{T,NOCT}$), 20 °C ambient temperature $T_{a,NOCT}$, and open-circuit conditions. For the PV module in this study, $T_{c,NOCT}$ is 45 °C. HOMER assumes $\tau\alpha$ = 0.9, following the recommendation by Duffie and Beckman [35]. The model also assumes that PV modules operate at the maximum power point, so the cell efficiency η_c corresponds to the maximum power point efficiency.

2.3.2. Wind Turbine Model

In this study, the Eocycle EOX S-16 wind turbine model, available in the HOMER library, was utilized [34]. The turbine has a rated power of 30 kW, with a reference height (h_{ref}) of 10 m and a hub height (h_{hub}) of 23.8 m. To determine the wind turbine's output power at each one-hour time step, HOMER first calculates the wind speed at the hub height (V_{hub}).

This calculation is performed using the logarithmic law, which considers wind speed at the reference height (V_{ref}), h_{hub}, h_{ref}, and surface roughness length (l_{sr}), as expressed in the following Equation (3):

$$V_{hub}(t) = V_{ref}(t) \times \frac{ln(h_{hub}/l_{sr})}{ln(h_{ref}/l_{sr})} \quad (3)$$

The wind speed value obtained at hub height (V_{hub}) is then applied to the wind turbine power curve to determine the output power at each time step. If the wind speed at hub height falls outside the operational range defined by the turbine's power curve, that is, below the cut-in speed or above the cut-out speed, the turbine is assumed to produce no power. This is one of the fundamental assumptions applied by HOMER throughout the simulation.

Additionally, to better reflect actual environmental conditions, HOMER adjusts the theoretical power output (P_{wt_pcurve}) derived from the power curve by applying an air density correction. The actual wind turbine output power (P_{wt_pcurve}) is calculated using Equation (4) below:

$$P_{wt\_out} = P_{wt\_pcurve} \times \left(\frac{\rho}{\rho_{std}}\right) \quad (4)$$

Here, ρ represents the actual air density (kg/m^3), while ρ_{std} refers to the standard air density (1.225 kg/m^3). This correction enables a more realistic representation of system performance under varying altitude and temperature conditions.

2.3.3. PHS Model

In this study, in addition to batteries and a hydrogen-based backup system, a PHS system is also integrated to store excess energy generated by renewable energy sources such as PV panels and WT. The PHS system operates by using surplus electricity to pump water from a lower reservoir to an upper reservoir, effectively converting electrical energy into gravitational potential energy. During periods when the generated energy and other backup components are insufficient to meet the load demand, the stored water is released from the upper reservoir to flow back into the lower reservoir through a turbine-generator unit. This process reconverts the potential energy into electricity, thereby compensating for energy deficits in the system.

In this coastal hotel case study, the sea is considered as the natural lower reservoir, which avoids the need for extensive excavation and makes the proposed PHS configuration more practical for Mediterranean coastal regions. Although seawater-based PHS systems are often criticized for corrosion challenges, operational experience from the Okinawa Yanbaru seawater PHS station has demonstrated the feasibility of pump-turbines operating successfully in saline conditions [36,37].

In HOMER, the PHS component is modeled using an idealized energy storage approach. In this framework, only key parameters such as maximum storage capacity (kWh), round-trip efficiency, and maximum output/input power (kW) are required. These values were calculated based on fundamental hydroelectric principles. Specifically, the maximum energy storage capacity of the upper reservoir was estimated using Equation (5) [38]:

$$E_{PHS}(kWh) = \frac{\rho \times g \times V \times h \times \eta}{3.6 \times 10^6} \quad (5)$$

In Equation (5) ρ is the density of water (1000 kg/m^3), g is the gravitational acceleration (9.81 m/s^2), V is the volume of the reservoir (m^3), h is the elevation difference between the upper and lower reservoirs in meters (m), and η is the overall efficiency, including turbine and generator losses. Similarly, the maximum power output was determined using the maximum flow rate Q (m^3/s), through Equation (6) [38]:

$$P_{PHS}(kW) = \frac{\rho \times g \times h \times Q \times \eta}{1000} \quad (6)$$

In this study, the PHS system is characterized based on fundamental hydroelectric principles. The system assumes a reservoir volume of 1000 m^3 and a practical head height of 100 m. Several studies in the literature have investigated low-head pumped hydro energy storage systems with head heights ranging from 20 to 100 m. Micro- and pico-scale PHS case studies, as summarized in [39], demonstrate that reservoir volumes between 80 and 1000 m^3 and head heights of approximately 20–100 m are both technically and economically feasible. In addition, Hoffstaedt et al. [40] provide a comprehensive review of low-head PHS technologies, highlighting the technical applicability and economic viability of systems operating within this head range. These findings, together with the demonstrated corrosion control experience from existing seawater PHS plants, indicate that the proposed seawater-based PHS configuration is consistent with reported literature and can be considered a technically, structurally, and practically feasible solution for integrating renewable energy sources in coastal regions.

Considering a combined turbine-generator efficiency of 90%, the system is capable of delivering approximately 20.44 kW of power during discharging, resulting in a total electrical energy output of 245.25 kWh over a 12-h discharge period. During the charging phase, the generator operates in reverse as a pump with the same efficiency, requiring approximately 14.8 h to refill the upper reservoir. The total energy input required for pumping is 302.7 kWh, which reflects the system's round-trip efficiency. Taking into account the pumping energy (input) and the generator output energy, the round-trip efficiency (η_{RT}) is formally defined as the ratio of the energy output to the energy input, as given in Equation (7):

$$\eta_{RT} = \frac{E_{out}}{E_{in}} = \frac{245.25\ \text{kWh}}{302.7\ \text{kWh}} = 0.81 \tag{7}$$

The elevation data of the coastal area at the proposed site were obtained using Google Earth Pro [41]. As illustrated in Figure 6, the terrain elevation increases to approximately 100 m within a horizontal distance of about 1.52 km from the coastline, resulting in an average coastal slope of 19.5% (maximum 20.5%). This gradient confirms that a 100 m head is topographically achievable within a short inland distance, ensuring the technical feasibility of the proposed seawater-based PHS configuration. The upper reservoir location therefore remains sufficiently close to the coast to maintain a moderate penstock length and a reasonable construction footprint.

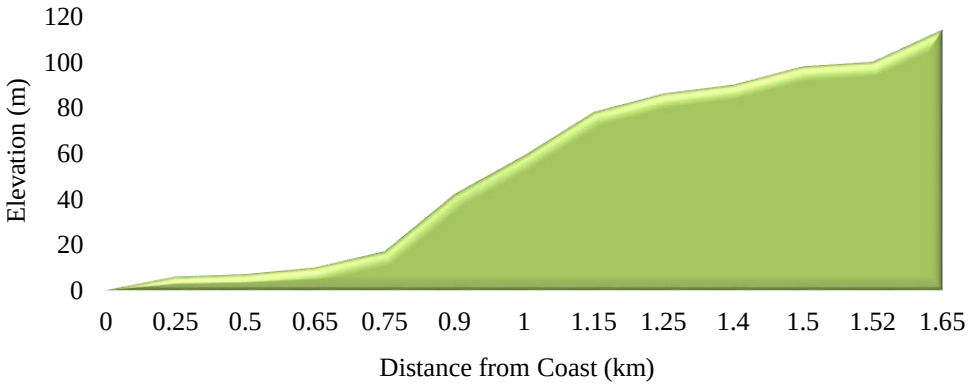

Figure 6. Elevation profile along the selected path from the Çenger/Manavgat shoreline.

This design approach is consistent with coastal seawater PHS studies such as Dufo-López et al. [21], who reported a 250 m head difference and 1.6 km distance between the reservoirs, as well as Ruiz et al. [37], who reported studies on seawater intake locations ranging from 20 to 635 m from the coast, corresponding to head differences between 142 and 605 m. These comparable case studies support the technical plausibility of the selected PHS

parameters for the Manavgat coastal region. Based on these site-specific considerations, the next step is to determine the appropriate penstock diameter to ensure efficient water flow between the upper and lower reservoirs.

The penstock diameter was estimated using the continuity relation between volumetric flow and velocity [42,43]:

$$D = \sqrt{\frac{4 \cdot Q}{\pi \cdot v}} \tag{8}$$

where D is the internal pipe diameter (m) and v is the mean flow velocity (m/s). Based on the reservoir volume of 1000 m^3, the average volumetric flow during the charging and discharging phases is $Q_{charge} = 0.01875$ m^3/s and $Q_{discharge} = 0.02315$ m^3/s, respectively. Since the same penstock is used for both directions, the penstock should be sized according to the higher flow rate. Assuming a typical mean velocity of approximately 2 m/s for small hydro penstocks, as recommended by European Small Hydropower Association (ESHA) [44] and applied in [45], the corresponding diameter is ≈ 0.12 m. This analytical estimation confirms that a compact penstock can accommodate both charging and discharging flows without introducing substantial head losses.

HOMER Pro calculates head losses due to penstock friction and includes turbine/pump efficiencies in the PHS module. For the physical implementation of the seawater PHS system, steel penstocks with roughness values of 0.045–0.05 mm were assumed, following typical design practice in coastal PHS systems [21,33]. While steel provides basic structural integrity, additional protective measures may be needed for long-term corrosion resistance. Such measures can slightly increase penstock costs, but their impact on the total system NPC is minimal due to the small share of piping infrastructure.

2.3.4. Battery Storage Model

In the hybrid energy system model, a generic lithium-ion battery with a nominal storage capacity of 100 kWh was utilized to balance the intermittent nature of renewable energy sources and improve system reliability. A nominal battery capacity of 100 kWh was selected based on the hotel's daily electrical load of 1505 kWh and peak demand of 123.47 kW. This sizing ensures adequate short-term load coverage while maintaining a cost-effective storage solution. Selecting a smaller-capacity battery would require a larger number of units to meet the same storage requirements, leading to higher investment costs and less efficient system operation.

According to the HOMER software database, the selected battery model operates at a nominal voltage of 600 V and has a nominal capacity of 167 Ah. The round-trip efficiency of the storage system, which reflects the ratio of energy retrieved during discharge to the energy used during charging, was assumed to be 90%.

The maximum allowable charge current was set to 167 A, while the maximum discharge current was defined as 500 A, ensuring the battery can respond effectively to both moderate and high load variations. The minimum state of charge (SOC) was constrained to 20% to prevent deep discharges that could shorten battery life, while the initial SOC at the beginning of the simulation was set to 100%.

When the total electrical power supplied by the system exceeds the load demand, the battery bank operates in charging mode. Conversely, when the system cannot fully meet the demand, the battery discharges to compensate for the power deficit. The energy stored in the battery at time t, denoted as $E_b(t)$, is updated using Equation (9), which simultaneously captures both charging and discharging dynamics [46]:

$$E_b(t) = E_b(t-1) \times (1-\alpha) + \left(P_{sist}(t) - \frac{P_{load}(t)}{\eta_{con}} \right) \times \eta_{bat} \tag{9}$$

In Equation (8) $E_b(t-1)$ represents the battery energy at the previous time step, α is the hourly self-discharge rate, $P_{sist}(t)$ and $P_{load}(t)$ are the total generated power and load demand at time t, respectively, η_{con} is the converter efficiency, and η_{bat} is the battery charging efficiency. A positive value of the term in parentheses corresponds to surplus generation, leading to battery charging, while a negative value indicates a power deficit, resulting in battery discharging. This single expression thus unifies both operational modes while incorporating energy conversion losses and self-discharge. Although the hourly self-discharge rate (α) is theoretically incorporated into the battery energy balance equation, HOMER software does not explicitly account for this loss unless a non-zero value is specified by the user. In this study, the default configuration is retained; therefore, the self-discharge effect is assumed to be negligible.

2.3.5. Fuel Cell Model

Fuel cells are electrochemical devices that generate electricity and heat by combining hydrogen with atmospheric oxygen. In the proposed hybrid energy system, hydrogen is produced from surplus renewable electricity via an electrolyzer. When the system operates in coordination with PHS, the energy management strategy prioritizes storing hydrogen over supplying it directly to the fuel cell. The amount of hydrogen consumed by the fuel cell ($Cons_{H_2}$) during time interval t is calculated using Equation (10) [47].

$$Cons_{H_2} = fcic \times P_{fc\_r} + fcs \times P_{fc}(t) \tag{10}$$

Here, $fcic$ is the fuel cell's intercept coefficient (kg/h per kW of rated power), and fcs is the slope coefficient (kg/h per kW of output). P_{fc_r} is the rated power of the fuel cell, and $P_{fc}(t)$ is the actual power it generates at time t. In this study, $fcic$ and fcs are taken as 0.0003 kg/h/kW and 0.0580 kg/h/kW, respectively. In the simulations, the PEM fuel cell was operated with a minimum load ratio of 30% to avoid deep discharges and extreme operating conditions that could accelerate performance degradation.

During the electrochemical conversion in proton exchange membrane fuel cells (PEMFCs), a significant amount of heat is released due to reversible electrochemical reactions, ohmic losses, reaction irreversibilities, and water vapor condensation. Normally, this non-negligible heat is dissipated into the air through cooling systems, limiting the hydrogen utilization efficiency to around 50%. Making effective use of this waste heat is an important research direction, and CHP is one of the most common approaches to achieve this [48].

In the proposed system, a portion of the fuel cell waste heat is recovered and transferred to the boiler as thermal energy, contributing to the system's thermal load coverage and enabling partial CHP operation.

The instantaneous electrical efficiency of the fuel cell, $\eta_{fc}\ (t)$, is calculated based on the hydrogen consumption, using the lower heating value of hydrogen (LHV_{H_2}), assumed to be 33.3 kWh/kg, as shown in Equation (11) [49,50]:

$$\eta_{fc}(\%) = \frac{P_{FC}}{LHV_{H_2} \times Cons_{H_2}} \times 100 \tag{11}$$

The recoverable thermal power output from the fuel cell, $P_{FC_{thr}}$, is then determined using Equation (12) [51,52]:

$$P_{FC\_thr} = Cons_{H_2} \times (1 - \eta_{fc}) \times LHV_{H_2} \times \eta_{HR} \tag{12}$$

where $Cons_{H_2}$ is the hydrogen consumption rate (kg/h), and η_{HR} is the heat recovery ratio. In this study, η_{HR} is assumed to be 60%, consistent with the default values used in HOMER. This fraction represents the portion of waste heat that can be effectively used for ther-

mal applications. Comparable recovery potentials have been reported for PEMFC-based CHP systems [53,54].

To account for the dynamic interaction between the recovered heat and the thermal load, a time-dependent allocation mechanism is introduced. The effective recovered heat utilized to meet the building's instantaneous thermal demand, $Q_{HR}(t)$, is defined as:

$$Q_{HR}(t) = \min(P_{FC_{thr}}(t),\ Q_{load_{thr}}(t)) \tag{13}$$

where $Q_{load_{thr}}(t)$ represents the thermal demand at time t. Any surplus waste heat that cannot be utilized is expressed as:

$$Q_{HR}(t) = \min(P_{FC_{thr}}(t),\ Q_{load_{thr}}(t)) \tag{14}$$

This formulation ensures that the waste heat is recovered only when the building's thermal demand exists, while any unutilized portion is treated as excess heat loss.

2.3.6. Electrolyzer and Hydrogen Tank Models

The electrolyzer and hydrogen tank models are implemented based on the approach used in the HOMER software environment [55]. In this system, the electrolyzer converts surplus electrical energy into hydrogen with a fixed efficiency of 85%. The produced hydrogen is stored in a pressurized tank and used later by the fuel cell when there is a power deficit. The initial hydrogen tank level is set to 10% of its total storage capacity.

In addition, the boiler and converter components are modeled with fixed efficiencies of 80% and 95%, respectively. The boiler is assumed to be an existing backup thermal component in the system and therefore is not associated with any capital cost, replacement cost, or lifetime constraints in the model. Its operation is based solely on the natural gas price specified in the financial assumptions.

2.4. Technical and Economic Parameters of Components

The technical and economic specifications of the components used in the HRES are summarized in Table 2. The table includes each component's rated power, capital and replacement costs, operation and maintenance expenses, and lifetime, based on relevant literature sources.

Table 2. Technical and economic parameters of the system components.

Component	Type	Capacity	Capital Cost ($)	Replacement Cost ($)	Operation & Maintenance Cost	Lifetime	Refs.
PV	SunPower E20-327	1 kW	1300	1300	20 $/year	25 years	[56]
WT	Eocycle EOX S-16	30 kW	60,000	54,000	500 $/turbine/yr	30 years	[57]
PHS	Generic 245 kWh	22 kW	22,000	500	100 $/year	25 years	[34,56]
Fuel cell	Generic	1 kW	3000	2500	0.01 $/h	50,000 h	[58,59]
Electrolyzer	Generic	1 kW	1500	1000	20 $/year	15 years	[60,61]
Hydrogen tank	Generic	1 kg	1300	1200	15 $	25 years	[62]
Battery	Generic 100 kWh Li-Ion	100 kWh	28,000	28,000	500 $/year	20 years/ 300,000 kWh	[20]
Boiler	Generic	-	-	-	-	25 years	[63]
Converter	Generic	1 kW	300	300	-	15 years	[49]

PV degradation is set to 0%/year in the current study, according to the Multi-Year Inputs settings in HOMER Pro. Wind turbine capacity is assumed to be constant over its lifetime (0% annual degradation), as commonly adopted in the literature. Battery degradation is considered through the specified lifetime and replacement cost.

3. Objective Function

In this study, the sizing optimization of PHS integrated HRES was performed under a set of technical and economic constraints using HOMER software. Among the various HRES configurations, the optimal system structure was identified based on the minimum NPC. The NPC represents the total expenditure related to installing and operating the system over its entire lifespan. These costs are adjusted to their present value using the real discount rate. The calculation encompasses capital investments, component replacements, operation and maintenance expenses, while also considering the salvage value of system components at the end of the project. Each component's NPC is derived from the present value of its expected cost streams. Accordingly, the objective function focuses on minimizing the overall NPC, formulated as the sum of annualized capital cost (AC_{cap}), annualized replacement cost (AC_{rep}), and annualized operation and maintenance ($AC_{O\&M}$) costs, as expressed in Equation (15) [32].

$$\min NPC = \frac{AC_{cap} + AC_{rep} + AC_{O\&M}}{CRF} \tag{15}$$

The capital recovery factor (CRF) is used to convert the total NPC into an equivalent annualized costs over the project lifetime and is given by Equation (16) [60]:

$$CRF[r_{dr}, R] = \frac{r_{dr}[1 + r_{dr}]^R}{[1 + r_{dr}]^R - 1} \tag{16}$$

In Equation (11), r_{dr} is the real discount rate and R is the project lifetime in years. The real discount rate (r_{dr}) accounts for the effect of inflation and is calculated from the nominal discount rate ($r_{nominal}$) and inflation rate (fr), as given in Equation (17) [50–65]:

$$r_{dr} = \frac{r_{nominal} - fr}{1 + fr} \tag{17}$$

In addition to NPC, HOMER also evaluates the COE as a supplementary economic metric. COE represents the average cost of producing each kilowatt-hour of electricity over the system's lifetime and is calculated by Equation (18) where E_{served} is the total electrical load served by the system per year [56]:

$$COE(\$/kWh) = \frac{AC_{cap} + AC_{rep} + AC_{O\&M}}{E_{served}} \tag{18}$$

3.1. Constraints and Decision Variables

In this study, operational and design constraints were established to ensure system reliability and sustainability. For all scenarios, the annual capacity shortage was fixed at 0%, guaranteeing that the energy demand is fully met throughout the simulation period. Moreover, a minimum renewable energy fraction of 75% was imposed to encourage environmentally friendly system configurations.

The optimization considered a set of decision variables representing the sizes or quantities of all system components. Each decision variable was restricted within predefined ranges or selected from discrete values. Table 3 summarizes the types (continuous or discrete) and boundaries of these decision variables used in the optimization process.

Table 3. Decision variables and boundaries.

Component	Variable	Type	Range/Values	Unit
PV	P_{PV}	Discrete	125–140–200–250–300–400–500	kW
Wind turbine	P_{wt}	Discrete	0–3–5–10–15	unit
Grid	P_{grid}	Discrete	25–35–50	kW
PHS	P_{PHS}	Continuous	0–20	unit
Fuel cell	P_{fc_r}	Discrete	0–10–15–20–25	kW
Electrolyzer	P_{elc}	Discrete	0–10–15–20–25–30–40	kW
Hydrogen tank	P_{ht}	Discrete	0–3–4–5–7	kg
Battery	E_b	Continuous	0–100	kWh
Boiler	P_{boiler}	Continuous	Unlimited	kW
Converter	P_{conv}	Continuous	0–600	kW

3.2. Financial Assumptions

For the financial analysis, this study assumes a nominal discount rate of 6% alongside an annual inflation rate of 2%. Based on these figures, the real discount rate is calculated as 3.92% using Equation (17). These parameters are applied consistently throughout the computation of NPC and COE. Additionally, the electricity and natural gas prices incorporated in the model are based on up-to-date local market data. Table 4 summarizes the financial parameters used.

Table 4. Key financial parameters used in economic analysis.

Parameter	Value	Unit
Project lifetime	25	years
Discount rate	6	%
Inflation rate	2	%
Real discount rate	≈3.92	%
Grid electricity purchase price	0.12	\$/kWh
Natural gas price (for boiler use)	0.15	$\$/m^3$

4. Results and Discussion

The optimal configuration of the HRES was evaluated to meet both the electrical and thermal energy demands of a seaside hotel in Manavgat, Antalya. The system comprised PV panels, WT, fuel cells, electrolyzers, hydrogen tanks, PHS, batteries, converters, and boilers, with both grid-connected and off-grid operation modes considered.

Simulations were performed in HOMER Pro using a Load Following dispatch strategy, with predefined technical and operational constraints (as defined in Section 3.1). The optimization process, which minimized NPC, resulted in six system configurations that demonstrate balanced performance in terms of economic efficiency, reliability, and environmental impact. The component combinations of these configurations are summarized

in Table 5, with the corresponding technical, economic, and environmental performance indicators presented in Table 6.

Table 5. Component configurations of HRES under different cases.

Components	Case 1	Case 2	Case 3	Case 4	Case 5	Case 6
PV	✓	✓	✓	✓	✓	✓
WT	✓	✓	✓	✓	✓	✓
Fuel Cell	×	×	✓	✓	✓	×
Electrolyzer	×	×	✓	✓	✓	×
Hydrogen Tank	×	×	✓	✓	✓	×
PHS	✓	✓	✓	✓	×	×
Battery storage	×	×	×	×	✓	✓
Grid	✓	×	✓	×	✓	✓
Converter	✓	✓	✓	✓	✓	✓
Boiler	✓	✓	✓	✓	✓	✓

Table 6. Technical, economic, and environmental performance of optimal HRES configurations for each case.

	Case 1	Case 2	Case 3	Case 4	Case 5	Case 6
PV (kW)	250	250	250	250	300	250
WT (30 kW)	10	10	10	10	10	10
Fuel Cell (kW)	-	-	10	10	10	-
Electrolyzer (kW)	-	-	10	10	10	-
Hydrogen Tank (kg)	-	-	3	4	4	-
PHS (245 kWh) string	8	10	9	10	-	-
Battery	-	-	-	-	19	22
Grid	50	-	50	-	50	50
Converter	189.05	187.50	125.00	156.57	139	167
NPC ($)	1,326,962	1,370,273	1,370,176	1,406,142	2,027,252	2,027,022
COE ($/kWh)	0.1527	0.1577	0.1577	0.1619	0.2337	0.2336
Initial capital ($)	1,157,715	1,201,250	1,209,400	1,242,170	1,614,050	1,591,059
Operating cost ($/yr)	10,744.24	10,729.97	10,206.45	10,409.34	26,231.02	27,676.05
Renewable Fraction (%)	96.34	96.63	96.38	96.63	96.51	96.32
Total Electrical Production (kWh/yr)	791,986	790,307	791,938	790,432	888,042	792,053
Unmet Electric Load (%)	0.0488	0.0602	0.0513	0.0619	0.0561	0.0482
Excess Electricity (kWh/yr)	166,812	164,703	166,403	164,481	273,164	195,222
Excess Electricity (%)	21.1	20.8	21	20.8	30.8	24.6
CO_2 Emissions Reduction (ton/yr)	259	259.9	259.2	260.1	255.2	247.2
Boiler fuel consumption (m^3/kg)	2424	2424	2421	2423	2277	2424

Table 6 summarizes the key performance indicators of the six optimal HRES configurations, including the installed capacities of each system component, NPC, COE, initial capital cost, annual operating cost, renewable energy fraction, total electrical production,

unmet load percentage, excess electricity, boiler fuel consumption, and the estimated annual CO_2 emissions reduction. These indicators provide a comprehensive basis for comparing the alternative configurations and support the identification of cost-effective and environmentally reliable energy supply solutions for the hotel.

Case 2, which represents a grid-independent version of Case 1, shows a slightly higher NPC and COE, with increases of 3.26% and 3.27%, respectively. The renewable energy fraction remains nearly the same, with only a 0.31% difference. In terms of cost structure, Case 2 has a 3.76% higher initial capital cost and a slightly lower annual operating cost by 0.13%. These differences arise mainly from the absence of a grid connection in Case 2, which necessitates a greater degree of self-sufficiency. To meet the annual capacity shortage constraint without grid support, the PHS capacity in Case 2 was increased by 25% compared to Case 1. This adjustment helped maintain system reliability while enhancing energy autonomy, making Case 2 a more suitable solution for off-grid or remote applications where access to the grid is limited or not feasible.

Case 3 integrates a hydrogen subsystem consisting of a 10 kW fuel cell, 10 kW electrolyzer, and 3 kg hydrogen tank, together with a 12.5% larger PHS capacity compared with Case 1. These additions increase the NPC and COE by 3.26% and 3.27%, respectively. Although the initial capital rises by 4.46%, the annual operating cost decreases by 5.01%, indicating a modest improvement in operational efficiency. The renewable fraction (96.4%) and reliability are almost identical to those of Case 1. Thus, Case 3 enhances the system's energy management capability and operational autonomy, as the integration of hydrogen components allows more effective balancing between variable renewable generation and demand, with only a limited cost penalty.

Case 4 further reduces grid dependency while maintaining the same hydrogen-based components as Case 3. To meet the annual capacity-shortage constraint, the PHS capacity is increased by 11% and the hydrogen-tank capacity by 33% relative to Case 3. Consequently, compared to Case 3, the NPC and COE increase by 2.62% and 2.66%, respectively, while the initial capital and operating costs rise by 2.7% and 2.0% due to the enlarged PHS and hydrogen-tank capacities. Compared to Case 1, the NPC and COE are 5.97% and 6.02% higher, respectively. Although this configuration maintains nearly identical renewable fraction and reliability levels (96.6% and 0.06%), the higher costs make it suitable primarily for remote sites without grid access.

Case 5 differs from previous configurations by eliminating the PHS subsystem and relying instead on a 19 kWh battery bank along with larger renewable capacities (300 kW PV, 10 kW WT, 10 kW FC/Electrolyzer, 4 kg H_2 tank). Compared to Case 1, the NPC and COE increase by 52.8% and 53.0%, reaching 2.03 M$ and 0.23 $/kWh, respectively. The initial investment grows by 39%, and the annual operating cost more than doubles (144%) relative to Case 1 due to the enlarged renewable capacities and battery storage. Although the renewable fraction remains high (96.5%), the excess electricity rises to 30.8% (63.8% higher than Case 1), reflecting system over-sizing to satisfy reliability constraints. Therefore, Case 5 ensures reliable operation but at significantly higher costs in the absence of long-duration PHS storage.

Case 6 also excludes the PHS subsystem and relies solely on a 22 kWh battery while retaining a 50 kW grid connection. Compared with Case 1, the NPC and COE increase by approximately 53%, reaching 2.03 M$ and 0.23 $/kWh, respectively. The initial capital rises by 37%, and the annual operating cost nearly triples due to the higher cost of battery-based storage. The renewable fraction remains around 96.3%, while excess electricity increases to 24.6% (17% higher than Case 1), reflecting oversizing to meet the reliability constraint. Compared with the other battery-integrated configuration (Case 5), Case 6 exhibits similar techno-economic performance but achieves slightly lower excess electricity owing to its

larger battery capacity. Hydrogen-integrated configurations with PHS (Cases 3 and 4) exhibit lower NPC and COE values and improved energy management compared with battery-integrated systems (Cases 5 and 6), confirming the techno-economic advantage of combining hydrogen storage with moderate PHS scaling for hotel-scale applications. Furthermore, the direct comparison between Case 1 and Case 6 highlights the superior performance of the proposed PHS-based storage system over purely battery-based alternatives, particularly in terms of cost-effectiveness and reduced excess electricity losses.

Overall, among all configurations, the PHS-based systems (Cases 1–4) achieve the best techno-economic balance, offering lower costs and minimized excess electricity while maintaining high renewable utilization and reliability levels.

As summarized in Table 6, considering all configurations, PHS emerges as the most efficient and cost-effective storage option, ensuring economic, reliable, and environmentally sustainable operation of the hotel's HRES. The unmet electric load values, ranging from 0.048% to 0.062% across all cases, confirm the effectiveness of the implemented load-following strategy in maintaining high system reliability.

Figure 7 provides a detailed cost breakdown for each case, including capital, replacement, operation and maintenance, fuel, salvage, the total NPC, and the COE. Serving as a complementary visualization to Table 6, this figure enables a clearer comparison of the cost distribution among the six HRES configurations.

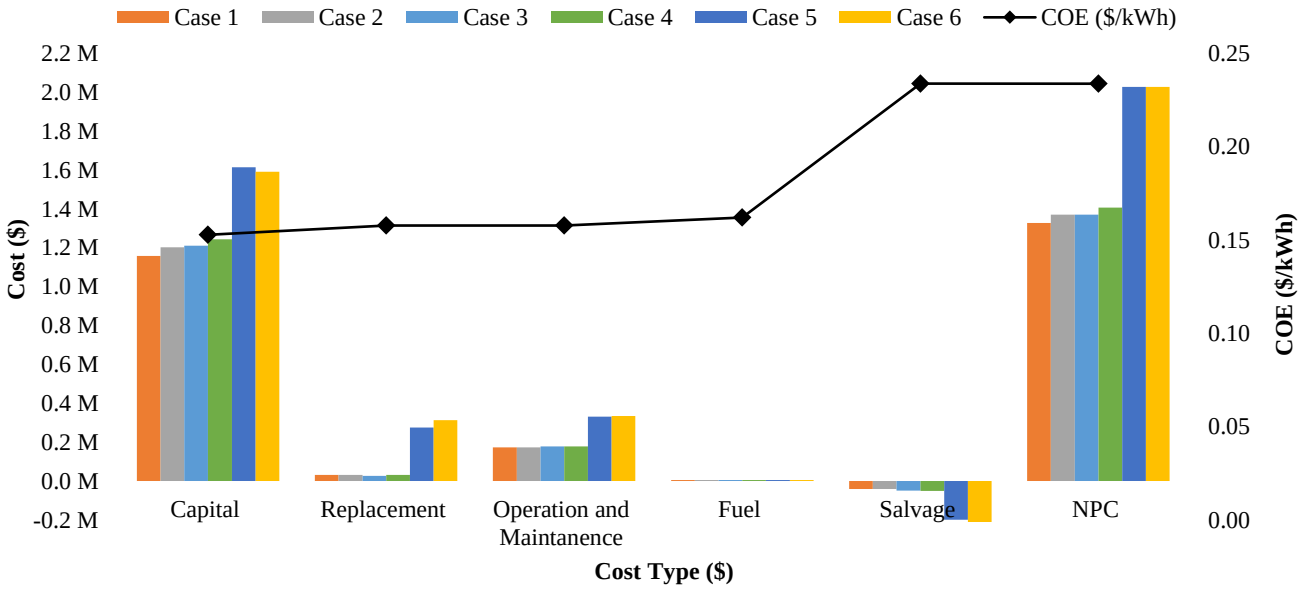

Figure 7. Comparison of cost types for six different cases.

It is clearly observed from Figure 7 that Case 1 emerges as the most cost-effective solution. Moreover, the first four HRES configurations, all of which utilize PHS as the main storage technology, exhibit relatively close values across all cost categories (i.e., capital, replacement, operation & maintenance, fuel, and salvage). In contrast, Cases 5 and 6 lead to significant increases across all cost components, including COE, as clearly illustrated in the figure.

4.1. Thermal Energy Management and Heat Recovery Performance

To better illustrate the role of heat recovery and the coordination between the fuel cell and boiler, Table 7 summarizes the annual thermal energy contributions for each configuration. The fuel cell contributes thermal energy through recovered waste heat,

which is first utilized to meet part of the heating demand and reduces the energy that must be supplied by the boiler, thereby lowering the boiler's fuel consumption.

Table 7. Annual thermal energy generation and distribution among system components.

Case	Fuel Cell Thermal Output (kWh/yr)	Fuel Cell Share (%)	Boiler Output (kWh/yr)	Boiler Share (%)	Excess Thermal (kWh/yr)	Excess Thermal (%)
1	–	–	19,151	100	–	–
2	–	–	19,151	100	–	–
3	113	0.588	19,125	99.4	87.1	0.455
4	71	0.37	19,138	99.6	57.8	0.302
5	4101	18.6	17,988	81.4	2938	15.3
6	–	–	19,151	100	–	–

Figure 8 presents the hourly variation in the thermal power during a representative period (21–22 November) for Case 3, corresponding to the optimum CHP configuration. When the thermal load ($Q_{load_{thr}}$) is active, the recovered heat from the fuel cell ($P_{FC_{thr}}$) is first utilized to partially meet the demand, and the remaining deficit is supplied by the boiler. This interaction demonstrates the temporal coordination between the two thermal sources and confirms.

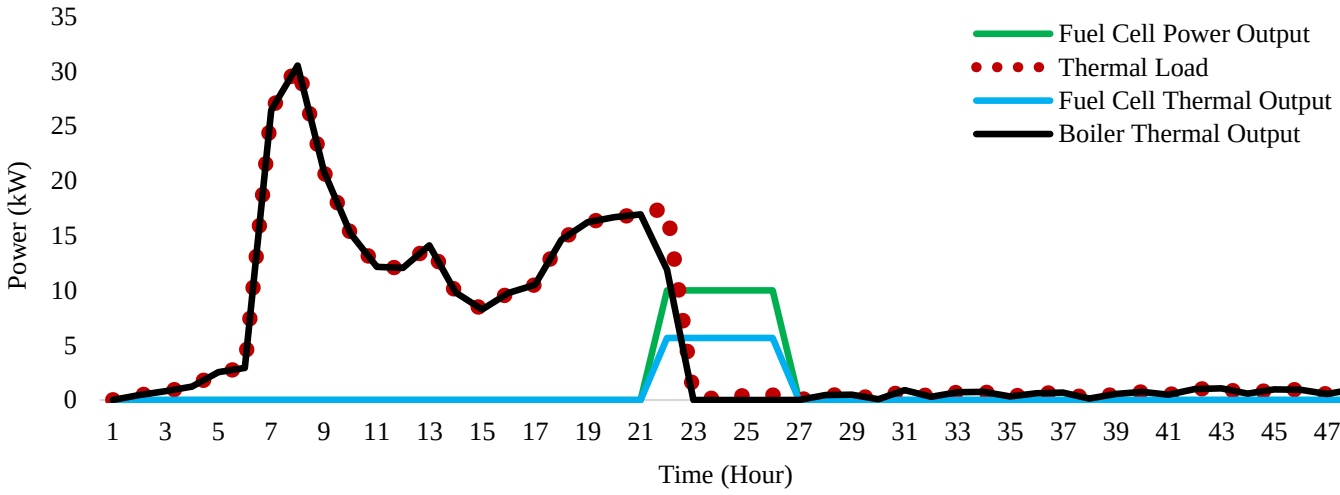

Figure 8. Power management simulation results for Case 3 during 21 and 22 November.

In addition to the representative hourly results for the optimum configuration (Case 3), Figure 9 presents the fuel cell CHP behavior for Case 5, which corresponds to the configuration without PHS but with both hydrogen and battery storage. Specifically, Figure 9a shows the annual variation in the fuel cell electrical output, while Figure 9b presents the fuel cell thermal output together with the boiler thermal output. In this configuration, the fuel cell operates more frequently when the hotel's electrical load increases and the total renewable generation (PV and wind) is insufficient to meet the demand. During spring and summer, this leads to higher fuel cell operation and increased recovered thermal energy, a significant portion of which becomes excess heat due to low thermal demand. In contrast, during winter months, when the thermal load is high, the fuel cell's recovered heat alone is insufficient, and the boiler supplements the deficit to ensure that the building's thermal

demand is fully satisfied. This figure thus illustrates the seasonal variation in recovered heat and the coordination between the fuel cell and boiler throughout the year.

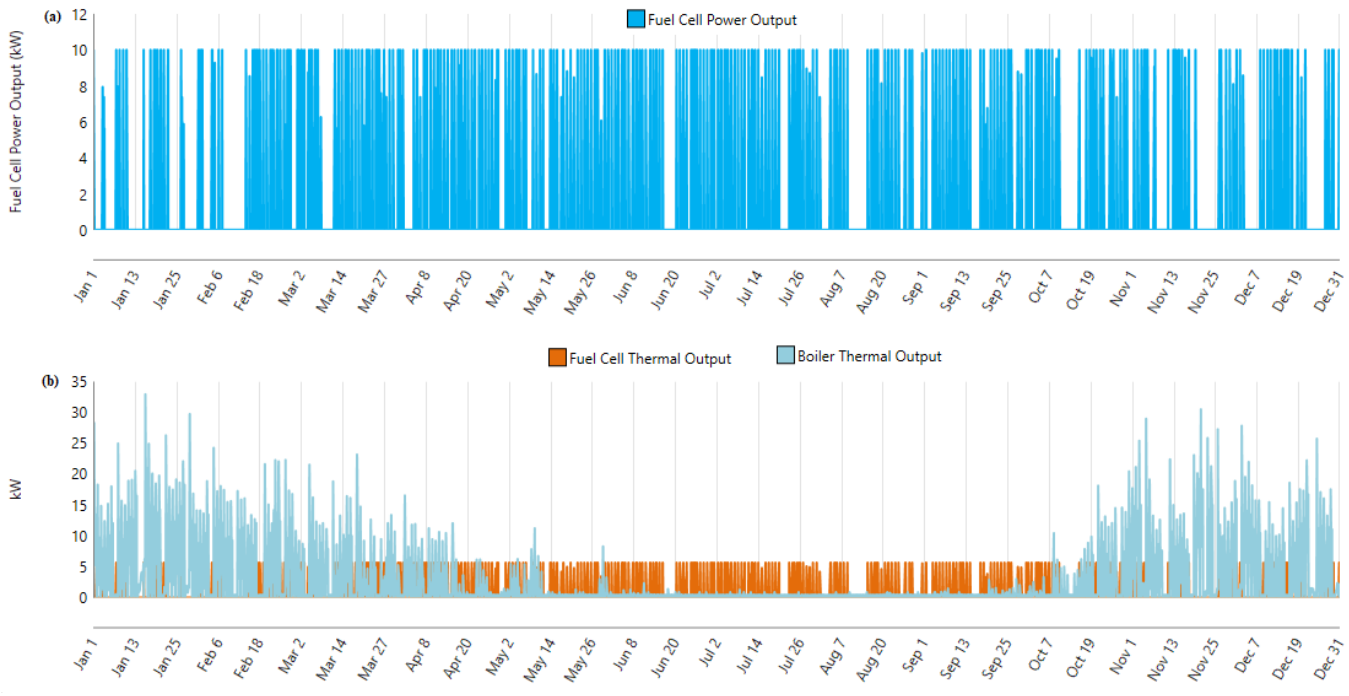

Figure 9. Annual performance of the fuel cell and thermal load balance in Case 5: (**a**) Annual fuel cell electrical output, (**b**) Annual fuel cell thermal output and boiler thermal output.

4.2. Optimum HRES Solution

Figure 10 presents the detailed cost breakdown of the system components for the optimal configuration identified in Case 1 among six different scenarios. According to Figure 10, the highest capital cost is attributed to the wind turbine, amounting to approximately $600,000, followed by the PV system with a capital cost of around $325,000, and PHS with $176,000.

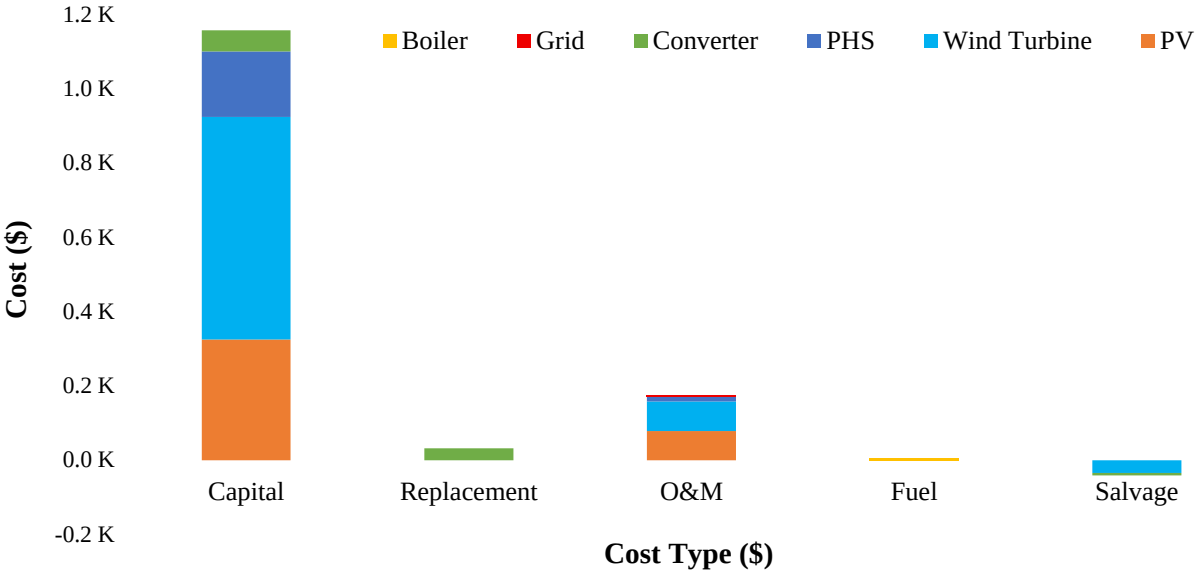

Figure 10. Comparison of cost types for Case 1.

In terms of operation and maintenance costs, PV and wind turbine systems collectively constitute the largest share, totaling approximately $78,761.98, while PHS contributes $12,601.92. Other components such as the boiler, grid, and converter have negligible or non-visible cost contributions in this scenario.

Figure 11 presents the monthly distribution of the system's electrical load alongside the contributions from PV, WT, PHS in both charge and discharge modes, and the grid. Over the course of the year, 56% of the total electricity generation was provided by PV, 43.8% by WT, and only 0.21% by the grid. Due to the characteristics of the Mediterranean climate, solar irradiation significantly decreases during the winter months, which explains why PV becomes the dominant electricity source in all months except November, December, and January. The PHS system actively operated in both charging and discharging modes throughout the year, contributing to energy balance, particularly by supplying additional power during periods of insufficient generation. Grid usage remained minimal, indicating that the system was largely self-sufficient. Overall, the distribution demonstrates a strong alignment between renewable energy generation and the load profile.

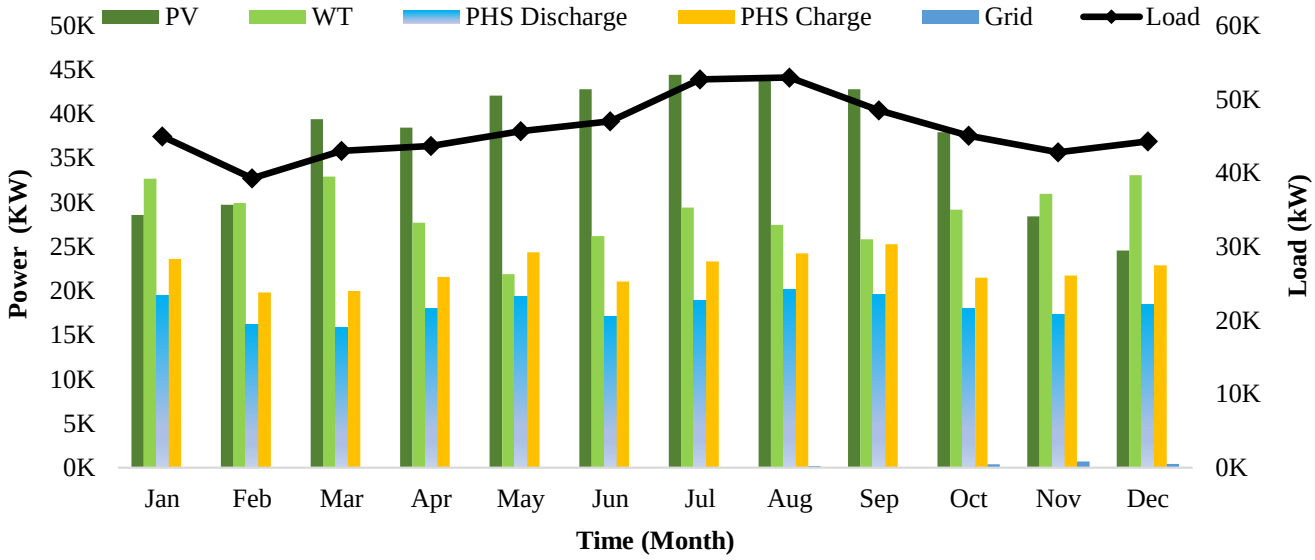

Figure 11. Monthly distribution of resource contributions to electricity demand in Case 1.

Figure 12 illustrates the power flow components for the first two days of April based on the PMS simulation results. The system prioritizes the use of renewable energy to meet the AC primary load, and excess energy is stored in the PHS unit. When renewable generation falls short of the demand, the PHS discharges to maintain supply continuity. Notably, the grid contribution remains negligible throughout the observed period, indicating the effectiveness of the proposed power management strategy in enabling autonomous system operation. This result highlights the importance of coordinated storage utilization to balance variability in renewable energy generation.

4.3. Sensitivity Analysis

4.3.1. The Impact of Real Discount Rate on NPC and COE

The economic performance of HRESs is highly sensitive not only to their technical configurations but also to the financial assumptions applied. In this context, the real discount rate plays a crucial role in evaluating the present value of all costs incurred throughout the entire lifetime of the system. It helps reduce the impact of inflation on long-term financial assessments, allowing for more accurate and realistic investment evaluations [66]. Since

the real discount rate may vary depending on overall economic fluctuations, it is regarded as a critical parameter that must be considered in sensitivity analyses [67].

In this study, the impact of real discount rate on NPC and COE was evaluated for six different system configurations. The goal is to assess the financial robustness of each configuration under varying economic conditions and to identify the most stable alternatives in terms of investment decisions. The real discount rate varied from 1.96% to 7.84%, corresponding to nominal discount rates between 4% and 10%, and its effect on both COE and NPC was analyzed for all system configurations (Figure 13). Results indicate that as the discount rate increases, COE generally rises, while NPC decreases, reflecting the reduced present value of future costs. Cases 1 and 2, which rely solely on PV, wind, and PHS (with or without grid backup), exhibit the lowest sensitivity, mainly because their configurations are simpler and involve fewer cost-intensive components. Cases 3 and 4, incorporating hydrogen technologies (fuel cell, electrolyzer, and H_2 tank) in addition to PHS, show slightly higher sensitivity, as the added hydrogen components increase both capital and replacement costs. However, their relatively small capacities limit the overall impact. Case 5, which integrates hydrogen storage alongside high-capacity PV and battery systems, displays moderate sensitivity, whereas Case 6, featuring only a large battery capacity but no hydrogen or PHS, exhibits the highest sensitivity due to the dominant influence of its large capital investments on both NPC and COE. Overall, systems with diversified storage types tend to be financially more robust under varying economic conditions than those relying solely on batteries.

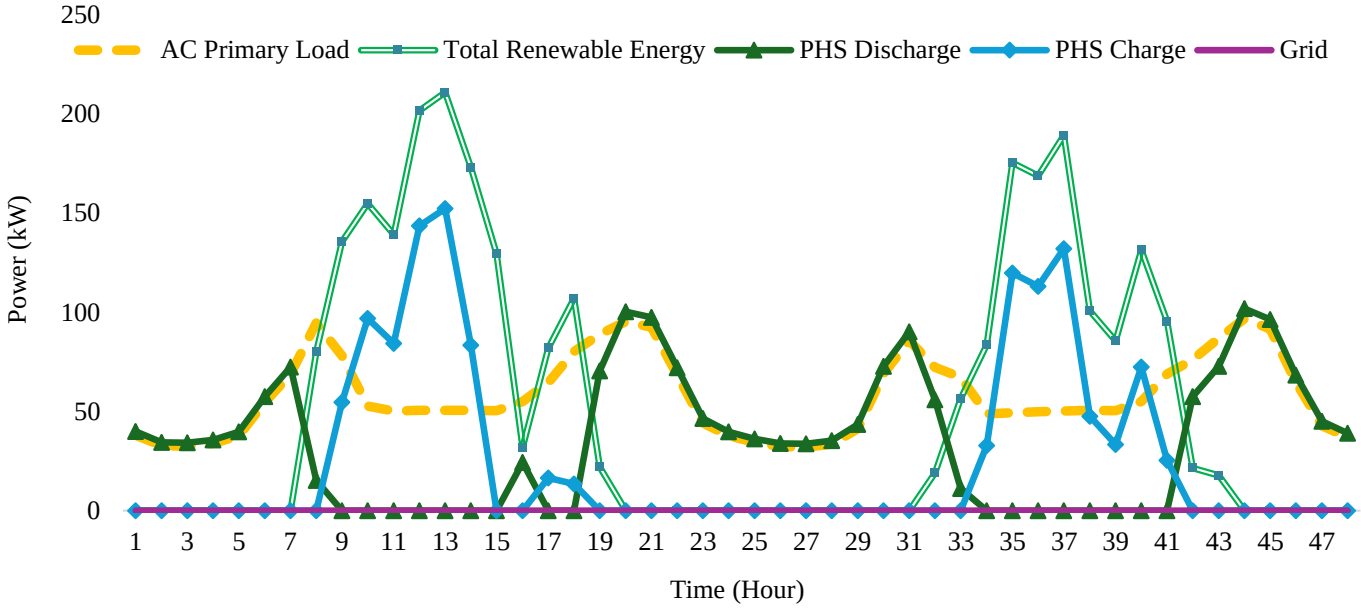

Figure 12. Power management simulation results for Case 1 during the first two days of April.

4.3.2. Sensitivity of NPC and COE to Component Costs in Case 1

The sensitivity analysis results for Case 1, presented in Figure 14, were conducted by varying the total costs of each component—including capital, operation and maintenance, and replacement—within a ±50–150% range, with the 100% baseline serving as the reference point. The results reveal distinct impacts of these cost variations on the system's NPC and COE. Among the components, WT demonstrate the highest sensitivity, with NPC and COE varying by approximately ±25% when WT total costs change by ±50%, indicating that system performance is particularly dependent on WT cost assumptions. PV systems show moderate sensitivity, with NPC and COE deviations ranging from −15% to +15%, suggesting that PV total cost fluctuations also significantly influence system economics.

In contrast, PHS exhibits relatively low sensitivity, with changes in NPC and COE within ±7%, highlighting the stabilizing role of PHS costs in overall system performance. Overall, the analysis indicates that reductions in WT and PV total costs could substantially decrease system costs, whereas PHS cost variations have only a limited effect. This outcome is consistent with the component sizing in Case 1, where WT and PV dominate the system investment, whereas PHS represents a smaller share of the total system cost. These findings emphasize the importance of prioritizing investment and policy measures targeting the more sensitive components to optimize the economic performance of HRESs.

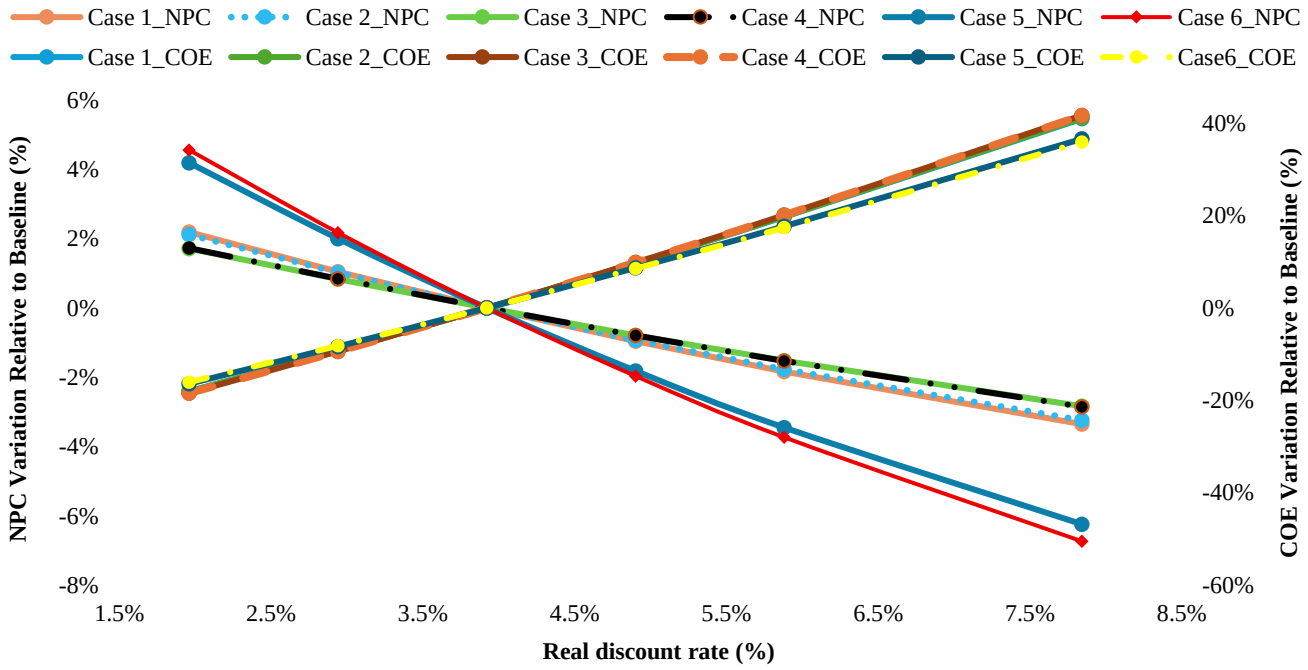

Figure 13. Effect of real discount rate on COE and NPC for different system configurations.

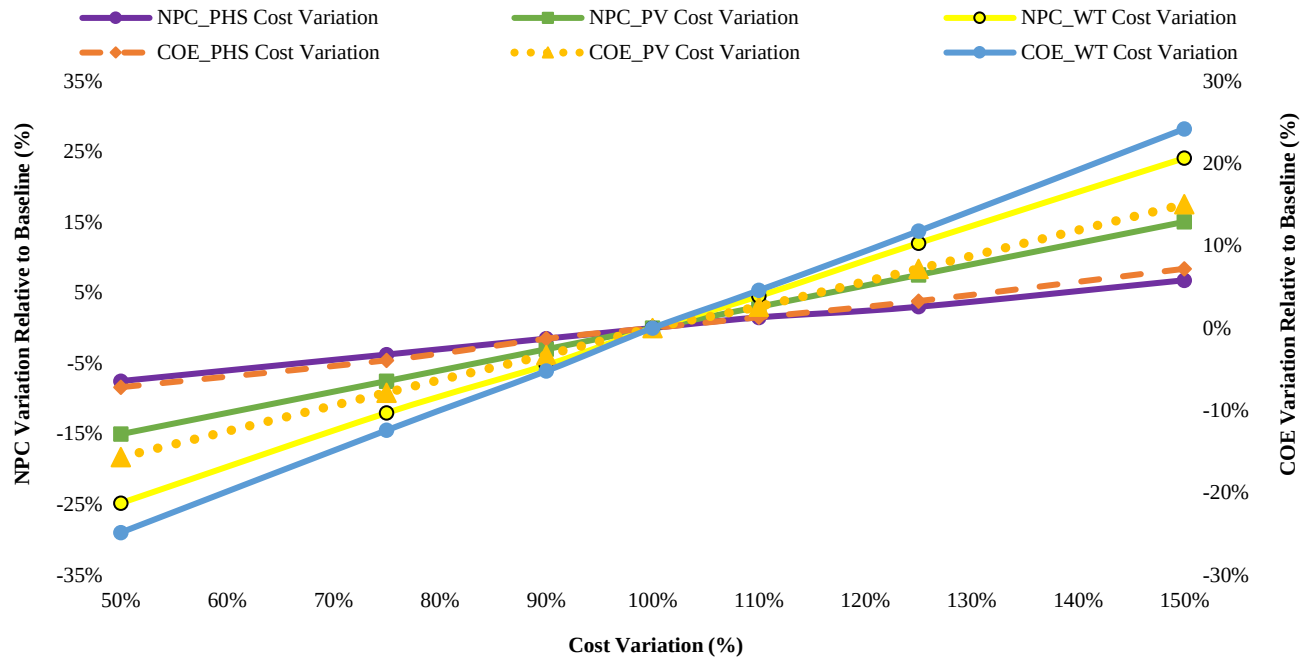

Figure 14. Relationship between cost variations of system components on NPC and COE (Case 1).

4.3.3. Sensitivity of NPC and COE to Storage Component Costs in Case 3

In Case 3, sensitivity analysis was conducted on the NPC and COE by varying the total costs of each component (including capital, operation and maintenance, and replacement) by ±50 relative to their baseline values (see Figure 15).

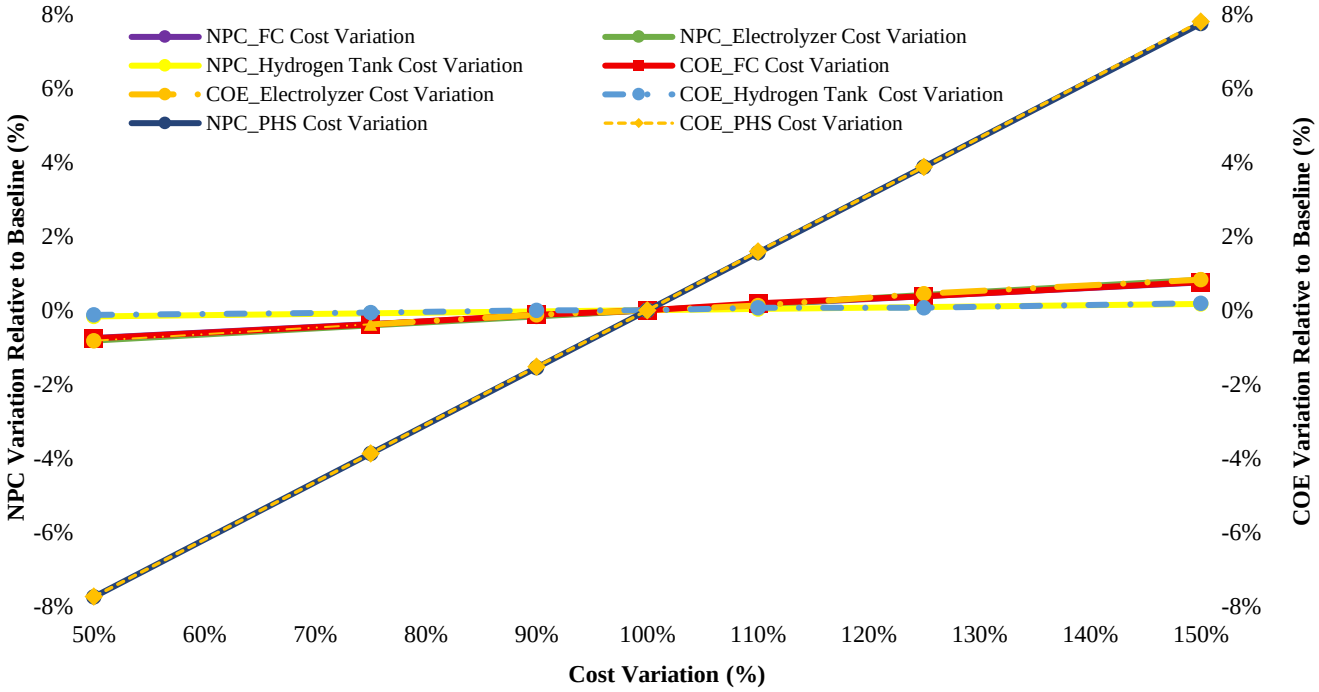

Figure 15. Effect of storage component cost variations on NPC and COE in Case 3.

The results reveal that the fuel cell (FC) and electrolyzer exert only marginal influence on the overall system economics, with maximum NPC and COE deviations of ±0.8%. The hydrogen storage tank shows an almost negligible impact, with changes of up to 0.2% in both NPC and COE. In contrast, PHS significantly affects the system performance, causing up to 7.7–7.8% increases in NPC and COE at the highest cost variation. These results indicate that the system's cost-effectiveness is predominantly governed by the PHS component, while the hydrogen-based subsystem has only a minor effect.

The observed sensitivity patterns are directly related to the relative sizes of the components in the optimal configuration (see Table 6). The FC (10 kW), electrolyzer (10 kW), and hydrogen tank (3 kg) were sized at relatively small capacities, resulting in very low contributions to the total system cost. Therefore, variations in their costs led to only minor changes in NPC and COE. On the other hand, PHS, with a total capacity of approximately 2.2 MWh (9 strings of 245 kWh each), represents the dominant storage unit in the system, accounting for a substantial portion of the total investment. Consequently, cost variations in PHS had the highest influence on the system economics, yielding the greatest sensitivity in both NPC and COE.

4.3.4. Sensitivity of NPC and COE to Load and Meteorological Parameters in Case 1

To evaluate the robustness of the optimal configuration (Case 1), a parametric sensitivity analysis was conducted by varying solar irradiance, ambient temperature, and wind speed by ±25%. The resulting impacts on NPC and COE are illustrated in Figures 16 and 17, respectively.

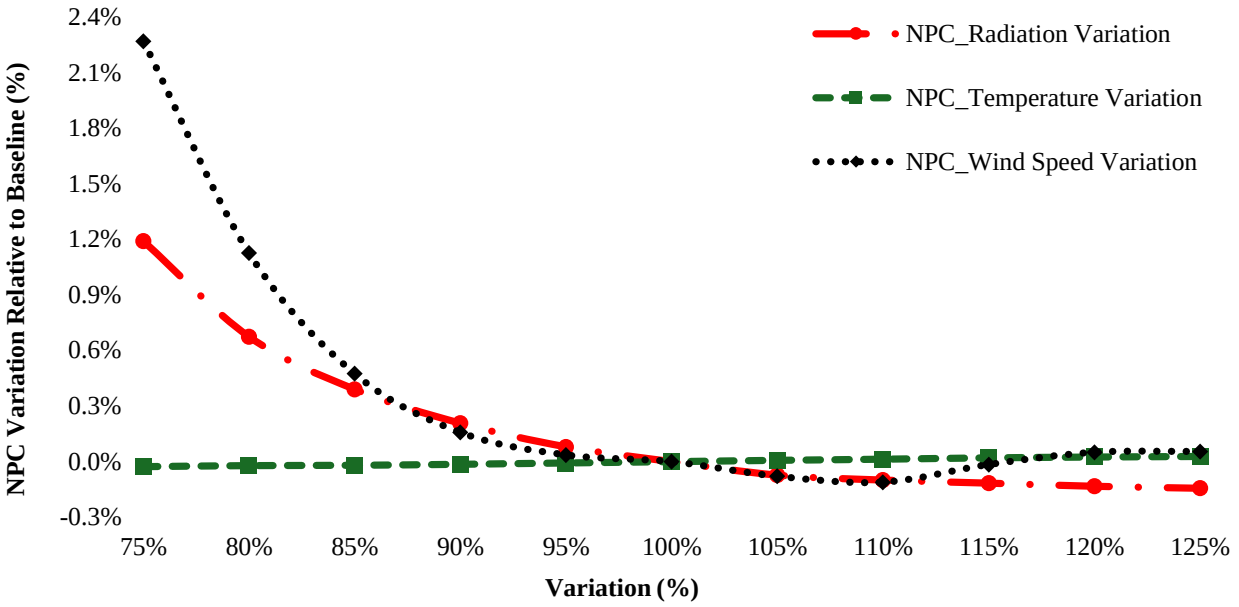

Figure 16. Sensitivity of NPC to variations in solar irradiance, temperature, and wind speed (Case 1).

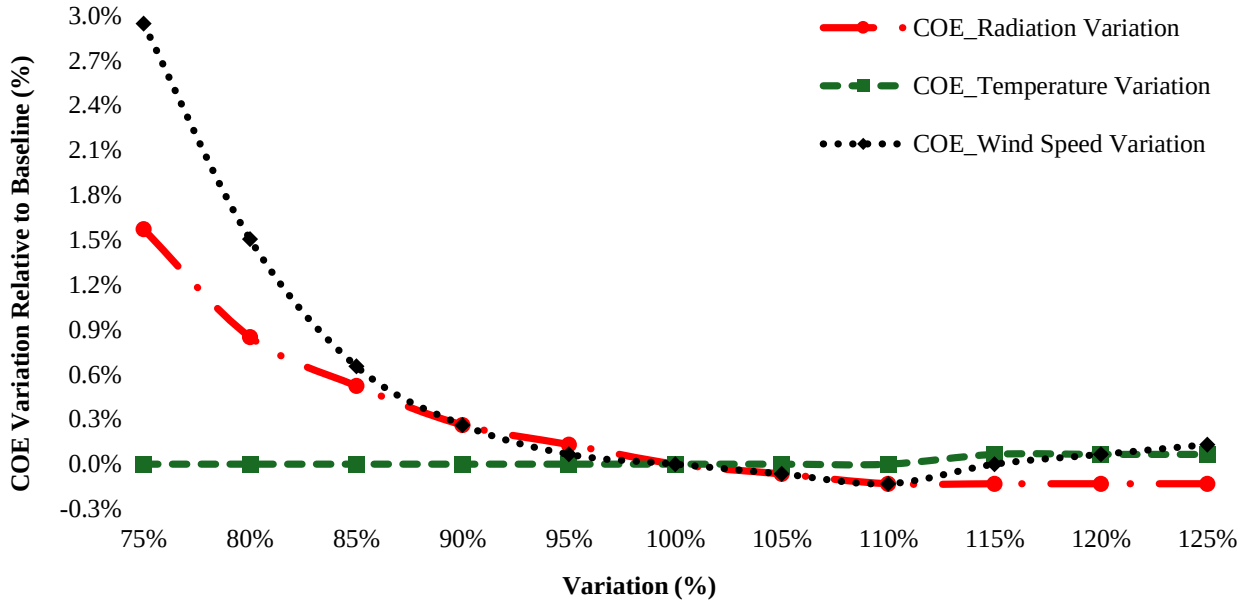

Figure 17. Sensitivity of COE to variations in solar irradiance, temperature, and wind speed (Case 1).

Among the tested parameters, wind speed has the strongest influence on techno-economic performance. A 25% reduction in wind speed increases NPC and COE by 2.27% and 2.95%, respectively, due to reduced renewable generation and higher grid dependence. Conversely, a 25% increase in wind speed slightly decreases NPC and COE by 0.06% and 0.13%, as the benefit of excess wind production is partially offset by limited storage capacity and minor curtailment during high-wind periods.

Solar irradiance shows a moderate effect. A 25% decrease raises NPC and COE by 1.19% and 1.57%, while a 25% increase reduces them by only about 0.13%. This limited improvement arises because the system cannot fully utilize the additional PV generation under fixed load and storage conditions, leading to small curtailment losses.

Ambient temperature has a negligible impact, with NPC and COE variations remaining within $\pm 0.03\%$, confirming the low thermal sensitivity of the PV subsystem under the studied climate.

Overall, the system exhibits robust techno-economic stability under moderate stochastic fluctuations in meteorological parameters, with wind speed identified as the dominant driver affecting both NPC and COE.

Figure 18 illustrates the impact of varying the system load from −25% to +25% on the NPC and COE. As the load increases, the NPC shows a moderate upward trend due to the higher energy production required to satisfy the additional demand and the increased reliance on the grid to compensate for renewable generation deficits. However, the COE decreases because the system's fixed and investment costs are distributed over a larger energy output. Conversely, when the load is reduced, the NPC slightly decreases due to the reduced use of the grid, which contributes a smaller share to the total energy supply. The COE, however, increases because the same fixed costs are allocated to a smaller amount of energy. Quantitatively, a 25% load reduction results in an approximate 33% increase in COE, whereas a 25% load increase leads to a 16% decrease in COE. In contrast, the total NPC varies only slightly over this load range, by approximately −0.24% to +3.43%. These results confirm that the COE is more sensitive to load fluctuations than the NPC.

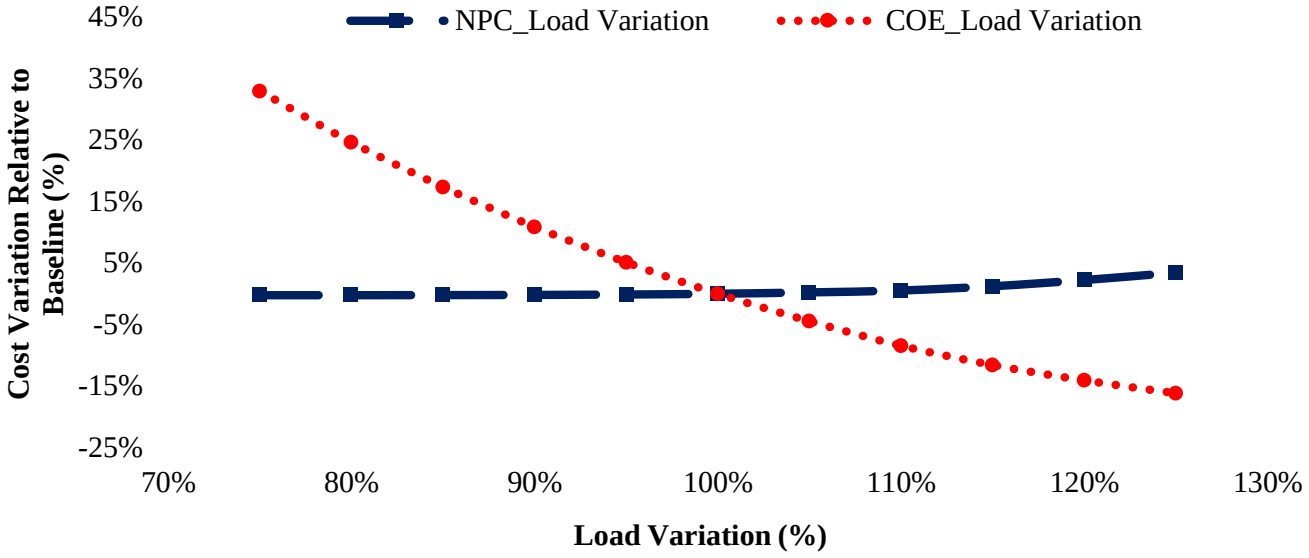

Figure 18. Effect of load variation (±25%) on NPC and COE (Case 1).

5. Conclusions

This study proposed the design and techno-economic optimization of an HRES for a seaside hotel in Manavgat, Antalya. The proposed system integrates PV panels, WT, PHS, hydrogen storage (via fuel cell, electrolyzer, and H_2 tank), batteries, and a boiler to meet both electrical and thermal energy demands under strict operational constraints, including 0% unmet load and a minimum renewable fraction of 75%. Both grid-connected and off-grid operation modes were considered to evaluate system flexibility and applicability in various scenarios.

Among the six configurations, the PHS-based system with grid support (Case 1) emerged as the most cost-effective solution, achieving an NPC of $1.33 million and a COE of $0.1527/kWh, while maintaining a renewable penetration of 96.34% and minimal excess electricity (21.1%). The off-grid PHS-based configuration (Case 2) and PHS–hydrogen storage systems (Cases 3–4) showed competitive performance with slightly higher costs. Cases 3–4 additionally provide complementary storage pathways and coordinated operation, contributing to waste heat utilization and system redundancy in case of component unavailability.

Battery-dominant systems without PHS (Cases 5–6) resulted in significantly higher initial capital costs (≈37–39%) and substantially higher COE values (≈53%), highlighting the cost and operational advantage of incorporating long-duration PHS. All PHS-based configurations maintained excess electricity at about 21%, while battery-dominant systems (Cases 5–6) experienced excess generation up to 31%, demonstrating the superior energy balancing capability of PHS.

The integration of renewable energy sources with storage components significantly reduces greenhouse gas emissions, with optimal configurations achieving up to 260 tons of annual CO_2 reduction compared to a fully grid-dependent baseline.

Sensitivity analyses indicate that PHS-based configurations provide financial robustness under varying real discount rate assumptions, while battery-only systems are more sensitive to real discount rate variations. Component cost sensitivity analysis confirms that WT and PV systems dominate system economics, whereas the PHS plays a stabilizing role and the hydrogen storage subsystem has a negligible impact due to its relatively small capacity. Load and meteorological variations primarily influence COE rather than total NPC, emphasizing the economic benefit of high renewable utilization and storage coordination. Overall, these findings demonstrate that combining PHS with optional hydrogen storage ensures a cost-effective, reliable, and environmentally sustainable HRES suitable for hotel-scale applications.

Funding: This research received no external funding.

Data Availability Statement: The data presented in this study are available on request from the corresponding author. (Additional detailed data from the study, which could not be included in the manuscript, are available from the corresponding author upon reasonable request).

Conflicts of Interest: The author declares no conflicts of interest.

References

1. Kilic, G.A.; Yalcin, E.; Aydin, A.A. Optimum Operating Temperature Range of Phase Change Materials Used in Cold Storage Applications: A Case Study. In *Environmentally-Benign Energy Solutions*; Dincer, I., Colpan, C.O., Ezan, M.A., Eds.; Springer International Publishing: Cham, Switzerland, 2020; pp. 711–726.
2. Akyuz, E.; Tezer, T. Techno-economic feasibility and regression analysis of green hydrogen production from solar and wind energy in Türkiye. *Int. J. Hydrogen Energy* **2025**, *142*, 1184–1195. [CrossRef]
3. Kılıç, G.A.; Al, K.; Dağtekin, E.; Ünver, Ü. Technical, economic and environmental investigation of grid-independent hybrid energy systems applicability: A case study. *Energy Sources Part A* **2020**, *47*, 461–476. [CrossRef]
4. Sun, C.; Zhang, H. Review of the development of first-generation redox flow batteries: Iron–chromium system. *ChemSusChem* **2021**, *14*, 4699–4721. [CrossRef] [PubMed]
5. Tezer, T.; Akyuz, E.; Gul, M. Optimal and reliable design of stand-alone hybrid renewable energy systems: A multi-objective approach. *Energy Sources Part A* **2024**, *46*, 10948–10963. [CrossRef]
6. Baumann, M.; Weil, M.; Peters, J.F.; Chibeles-Martins, N.; Moniz, A.B. A review of multi-criteria decision making approaches for evaluating energy storage systems for grid applications. *Renew. Sustain. Energy Rev.* **2019**, *107*, 516–534. [CrossRef]
7. Toufani, P.; Karakoyun, E.Ç.; Nadar, E.; Fosso, O.B.; Kocaman, A.S. Optimization of pumped hydro energy storage systems under uncertainty: A review. *J. Energy Storage* **2023**, *73*, 109306. [CrossRef]
8. Hosseini, S.E.; Dincer, I.; Rosen, M.A. Hybrid solar–fuel cell combined heat and power systems for residential applications: Energy and exergy analyses. *J. Power Sources* **2013**, *221*, 372–380. [CrossRef]
9. Zafar, S.; Dincer, I. Thermodynamic analysis of a combined PV/T–fuel cell system for power, heat, fresh water and hydrogen production. *Int. J. Hydrogen Energy* **2014**, *39*, 9962–9972. [CrossRef]
10. Devrim, Y.; Bilir, L. Performance investigation of a wind turbine–solar photovoltaic panels–fuel cell hybrid system installed at İncek region—Ankara, Turkey. *Energy Convers. Manag.* **2016**, *126*, 759–766. [CrossRef]
11. Pürlü, M.; Andiç, C.; Aydın, E.; Solak, B. Optimal design of hybrid renewable energy system for a region in Turkey using HOMER. *Turk. J. Electr. Power Energy Syst.* **2023**, *3*, 146–155. [CrossRef]

12. Pattnaik, A.; Dauda, A.K.; Panda, A. Optimal utilization of clean energy and its impact on hybrid power systems incorporating STATCOM and pumped hydro storage. *Renew. Sustain. Energy Rev.* **2023**, *187*, 113713. [CrossRef]
13. Ali, S.; Stewart, R.A.; Sahin, O. Drivers and barriers to the deployment of pumped hydro energy storage applications: Systematic literature review. *Clean. Eng. Technol.* **2021**, *5*, 100281. [CrossRef]
14. Anagnostopoulos, J.S.; Papantonis, D.E. Simulation and size optimization of a pumped–storage power plant for the recovery of wind-farms rejected energy. *Renew. Energy* **2008**, *33*, 1685–1694. [CrossRef]
15. Ma, T.; Yang, H.; Lu, L.; Peng, J. An optimization sizing model for solar photovoltaic power generation system with pumped storage. *Energy Procedia* **2014**, *61*, 5–8. [CrossRef]
16. Jurasz, J.; Dąbek, P.B.; Kaźmierczak, B.; Kies, A.; Wdowikowski, M. Large scale complementary solar and wind energy sources coupled with pumped-storage hydroelectricity for Lower Silesia (Poland). *Energy* **2018**, *161*, 183–192. [CrossRef]
17. Simão, M.; Ramos, H.M. Hybrid Pumped Hydro Storage Energy Solutions towards Wind and PV Integration: Improvement on Flexibility, Reliability and Energy Costs. *Water* **2020**, *12*, 2457. [CrossRef]
18. Gioutsos, D.M.; Blok, K.; van Velzen, L.; Moorman, S. Cost-optimal electricity systems with increasing renewable energy penetration for islands across the globe. *Appl. Energy* **2018**, *226*, 437–449. [CrossRef]
19. Guezgouz, M.; Jurasz, J.; Bekkouche, B.; Ma, T.; Javed, M.S.; Kies, A. Optimal hybrid pumped hydro-battery storage scheme for off-grid renewable energy systems. *Energy Convers. Manag.* **2019**, *199*, 112046. [CrossRef]
20. Samatar, A.M.; Lekbir, A.; Mekhilef, S.; Mokhlis, H.; Tey, K.S.; Alassaf, A. Techno-economic and environmental analysis of a fully renewable hybrid energy system for sustainable power infrastructure advancement. *Sci. Rep.* **2025**, *15*, 12140. [CrossRef]
21. Dufo-López, R.; Lujano-Rojas, J.M. Optimization of size and operation of stand-alone renewable-based systems with diesel and hybrid pumped hydro storage–battery storage considering uncertainties. *Batteries* **2025**, *11*, 70. [CrossRef]
22. Abdelshafy, A.M.; Jurasz, J.; Hassan, H.; Mohamed, A.M. Optimized energy management strategy for grid-connected double storage (pumped storage–battery) system powered by renewable energy resources. *Energy* **2020**, *192*, 116615. [CrossRef]
23. Ramos, H.M.; Sintong, J.E.; Kuriqi, A. Optimal integration of hybrid pumped storage hydropower toward energy transition. *Renew. Energy* **2024**, *221*, 119732. [CrossRef]
24. Taşcıkaraoğlu, A.; Erdinç, O. A profit optimization approach based on the use of pumped-hydro energy storage unit and dynamic pricing. *J. Eng. Archit. Fac. Eskiseh. Osman. Univ.* **2018**, *26*, 74–87.
25. Kocaman, A.S. Optimization of hybrid energy systems with pumped hydro storage: A case study for Turkey. *J. Fac. Eng. Archit. Gazi Univ.* **2019**, *34*, 53–67. [CrossRef]
26. Kumcu, Ş.Y. Pumped-hydro energy storage alternative site evaluation: A case study in Turkey. *J. Int. Environ. Appl. Sci.* **2019**, *14*, 70–74.
27. Saltuk, M.F. Prefeasibility analysis of the pumped hydro storage (PHS) system in Türkiye: A case study on a hybrid system. *Energy Storage Convers.* **2023**, *1*, 215. [CrossRef]
28. Yurter, G.; Nadar, E.; Kocaman, A.S. The impact of pumped hydro energy storage configurations on investment planning of hybrid systems with renewables. *Renew. Energy* **2024**, *222*, 119906. [CrossRef]
29. Ünver, Ü.; Bilgin, H.; Güven, A. Pompaj depolamalı hidroelektrik sistemler. *Mühendis Ve Makina* **2015**, *56*, 57–64.
30. Sertkaya, A.A.; Saraç, M.; Arslan, M.A.O. The importance of pumped-storage hydroelectric power plants for Turkey. *Gazi J. Eng. Sci.* **2015**, *1*, 369–382.
31. Gürsakal, H.; Uyumaz, A. Pompaj depolamalı hidroelektrik santrallerin optimizasyonunda kârlılık analizi ve çalışma süresi tayini. *Mühendislik Bilim. Tasar. Derg.* **2021**, *9*, 436–452. [CrossRef]
32. Awan, A.B.; Zubair, M.; Sidhu, G.A.S.; Bhatti, A.R.; Abo-Khalil, A.G. Performance analysis of various hybrid renewable energy systems using battery, hydrogen, and pumped hydro-based storage units. *Int. J. Energy Res.* **2019**, *43*, 6296–6321. [CrossRef]
33. Alili, H.; Mahmoudimehr, J. Techno-economic assessment of integrating hydrogen energy storage technology with hybrid photovoltaic/pumped storage hydropower energy system. *Energy Convers. Manag.* **2023**, *294*, 117437. [CrossRef]
34. HOMER Energy. *HOMER Pro, Version 3.14.2*; HOMER Energy, LLC: Boulder, CO, USA, 2017.
35. Duffie, J.A.; Beckman, W.A. *Solar Engineering of Thermal Processes*, 2nd ed.; Wiley: New York, NY, USA, 1991.
36. Oshima, K.; Kawai, J.; Otsuka, S.; Wada, T.; Imano, H. Development of Pump-Turbine for Seawater Pumped Storage Power Plant. In *Waterpower '99: Hydro's Future: Technology, Markets, and Policy, Proceedings of the International Conference on Hydropower, Las Vegas, NV, USA, 6–9 July 1999*; American Society of Civil Engineers (ASCE): Reston, VA, USA, 1999; pp. 1–6.
37. Ansorena Ruiz, L.H.; de Vilder, E.B.; Prasasti, M.; De Luca, A.; Geisseler, B.; Terheiden, K.; Scanu, S.; Miccoli, A.; Roeber, V.; Marence, M.; et al. Low-Head Pumped Hydro Storage: A Review on Civil Structure Designs, Legal and Environmental Aspects to Make Its Realization Feasible in Seawater. *Renew. Sustain. Energy Rev.* **2022**, *160*, 112281. [CrossRef]
38. HOMER Energy. *HOMER Help: Pumped Hydro, Version 3.14.2*; HOMER Energy, LLC: Boulder, CO, USA, 2017.

39. Majoral Oller, G. Anàlisi de Viabilitat de Salts Hidràulics Reversibles Tancats de Capacitat Mitjana i Petita per Emmagatzematge d'Energia/Feasibility Study on Closed-loop Small-Scale Pumped Hydro Energy Storage Systems. Master's Thesis, Universitat Politècnica de Catalunya, Barcelona, Spain, 26 June 2020. Available online: https://upcommons.upc.edu/server/api/core/bitstreams/17bc95ed-3130-4388-827d-3db8d3ee5cd8/content (accessed on 1 September 2025).
40. Hoffstaedt, J.P.; Truijen, D.P.K.; Fahlbeck, J.; Gans, L.H.A.; Qudaih, M.; Laguna, A.J.; De Kooning, J.D.M.; Stockman, K.; Nilsson, H.; Storli, P.-T.; et al. Low-head pumped hydro storage: A review of applicable technologies for design, grid integration, control and modelling. *Renew. Sustain. Energy Rev.* **2022**, *158*, 112119. [CrossRef]
41. Google LLC. *Google Earth Pro, Version 7.3.6.10441*; Google LLC: Mountain View, CA, USA, 2025; Çenger, Manavgat, Türkiye. Elevation data retrieved from the Google Earth Pro application.
42. Munson, B.R.; Young, D.F.; Okiishi, T.H.; Huebsch, W.W. *Fundamentals of Fluid Mechanics*, 7th ed.; Wiley: Hoboken, NJ, USA, 2013.
43. Kilic, G.A. Performance Evaluation of Triply Periodic Minimal Surface Heat Exchangers Using Nanofluids at High Flow Rates for Enhanced Energy Efficiency. *Appl. Sci.* **2025**, *15*, 4140. [CrossRef]
44. Penche, C. *Guide on How to Develop a Small Hydropower Plant*; European Small Hydropower Association (ESHA): Brussels, Belgium, 2004.
45. Tsuanyo, D.; Amougou, B.; Aziz, A.; Nnomo, B.N.; Fioriti, D.; Kenfack, J. Design models for small run-of-river hydropower plants: A review. *Sustain. Energy Res.* **2023**, *10*, 3. [CrossRef]
46. Maleki, A.; Askarzadeh, A. Comparative study of artificial intelligence techniques for sizing of a hydrogen-based stand-alone photovoltaic/wind hybrid system. *Int. J. Hydrogen Energy* **2014**, *39*, 9973–9984. [CrossRef]
47. Singh, S.; Chauhan, P.; Singh, N.J. Capacity optimization of grid connected solar/fuel cell energy system using hybrid ABC-PSO algorithm. *Int. J. Hydrogen Energy* **2020**, *45*, 10070–10088. [CrossRef]
48. Song, K.; Hou, T.; Jiang, J.; Grigoriev, S.A.; Fan, F.; Qin, J.; Wang, Z.; Sun, C. Thermal management of liquid-cooled proton exchange membrane fuel cell: A review. *J. Power Sources* **2025**, *648*, 237227. [CrossRef]
49. Budak, Y.; Devrim, Y. Investigation of micro-combined heat and power application of PEM fuel cell systems. *Energy Convers. Manag.* **2018**, *160*, 486–494. [CrossRef]
50. Tezer, T.; Yaman, R. A Pareto optimum approach and a power management strategy for a stand-alone wind turbine–PV–hydrogen with reformer hybrid renewable energy system. *Environ. Prog. Sustain. Energy* **2022**, *41*, e13772. [CrossRef]
51. Ren, F.K.; Wang, J.J.; Zhu, S.T.; Chen, Y. Multi-objective optimization of combined cooling, heating and power system integrated with solar and geothermal energies. *Energy Convers. Manag.* **2019**, *197*, 111866. [CrossRef]
52. Li, L.L.; Ren, X.Y.; Tseng, M.L.; Wu, D.S.; Lim, M.K. Performance evaluation of solar hybrid combined cooling, heating and power systems: A multi-objective arithmetic optimization algorithm. *Energy Convers. Manag.* **2022**, *258*, 115541. [CrossRef]
53. Nguyen, H.Q.; Shabani, B. Proton exchange membrane fuel cells heat recovery opportunities for combined heating/cooling and power applications. *Energy Convers. Manag.* **2020**, *204*, 112328. [CrossRef]
54. Mohamed, W.A.N.W.; Singh, B.; Mohamed, M.F.; Aizuwan, A.M.; Zubair, A.B.M. Effects of fuel cell vehicle waste heat temperatures and cruising speeds on the outputs of a thermoelectric generator energy recovery module. *Int. J. Hydrogen Energy* **2021**, *46*, 25634–25649. [CrossRef]
55. Lilienthal, P.; Lambert, T.; Gilman, P. Computer modeling of renewable power systems. *Encycl. Energy* **2004**, *1*, 633–647. [CrossRef]
56. Das, B.K.; Hasan, M.; Rashid, F. Optimal sizing of a grid-independent PV/diesel/pumped-hydro hybrid system: A case study in Bangladesh. *Sustain. Energy Technol. Assess.* **2021**, *44*, 100997. [CrossRef]
57. Akhtari, M.R.; Baneshi, M. Techno-economic assessment and optimization of a hybrid renewable co-supply of electricity, heat, and hydrogen system to enhance performance by recovering excess electricity for a large energy consumer. *Energy Convers. Manag.* **2019**, *188*, 131–141. [CrossRef]
58. Das, B.K.; Tushar, M.S.H.K.; Zaman, F. Techno-economic feasibility and size optimisation of an off-grid hybrid system for supplying electricity and thermal loads. *Energy* **2021**, *215*, 119141. [CrossRef]
59. Jamshidi, M.; Askarzadeh, A. Techno-economic analysis and size optimization of an off-grid hybrid photovoltaic, fuel cell and diesel generator system. *Sustain. Cities Soc.* **2019**, *44*, 310–320. [CrossRef]
60. Tezer, T. Multi-Objective Optimization of Hybrid Renewable Energy Systems with Green Hydrogen Integration and Hybrid Storage Strategies. *Int. J. Hydrogen Energy* **2025**, *142*, 1249–1271. [CrossRef]
61. Khan, T.; Ullah, Z.; Agyekum, E.B.; Hasanien, H.M.; Yu, M. Multi-objective optimization of combined heat and power system integrated with multi-energy storage systems for rural communities. *J. Energy Storage* **2024**, *99*, 113433. [CrossRef]
62. El Boujdaini, L.; Jurado, F.; Mezrhab, A.; Moussaoui, M.A.; Vera, D. Cost and size optimization of hybrid solar and hydrogen subsystem using HomerPro software. *Int. J. Hydrogen Energy* **2023**, *48*, 24018–24036. [CrossRef]
63. HOMER Energy. *HOMER Help: Boiler, Version 3.14.2*; HOMER Energy, LLC: Boulder, CO, USA, 2017.
64. Tehrani, M.M.; Akhtari, M.; Kasaeian, A.; Rad, M.A.V.; Toopshekan, A.; Motlagh, M.S. Techno-economic investigation of a hybrid biomass renewable energy system to achieve the goals of SDG-17 in deprived areas of Iran. *Energy Convers. Manag.* **2023**, *291*, 117319. [CrossRef]

65. Gül, M.; Akyüz, E. Hydrogen generation from a small-scale solar photovoltaic thermal (PV/T) electrolyzer system: Numerical model and experimental verification. *Energies* **2020**, *13*, 2997. [CrossRef]
66. Altunsoy, Ü. Kargo taşımacılık sisteminde elektrikli araçlar kullanımı üzerine inceleme. *Int. Anatolia Acad. Online J. Sci. J.* **2021**, *7*, 1–14.
67. Bilal, M.; Oladigbolu, J.O.; Mujeeb, A.; Al-Turki, Y.A. Cost-effective optimization of on-grid electric vehicle charging systems with integrated renewable energy and energy storage: An economic and reliability analysis. *J. Energy Storage* **2024**, *100*, 113170. [CrossRef]